STELLAR SURFACE STRUCTURE

ARSEN R. HAJIAN

AUGUST 13, '99

- UNIFORM DISKS
- LIMB-DARKENED DISKS
- ELLIPTICAL STARS
- SPOTS

UNIFORM DISKS

- 1st APPROXIMATION

- $$V^2 = \left| \frac{2\, J_1(x)}{x} \right|^2$$

  WHERE $x = \dfrac{\pi d \theta_{UD}}{\lambda_0}$

  THIS IS THE FAMILIAR AIRY FUNCTION

- OVER 400 UDDS EXIST

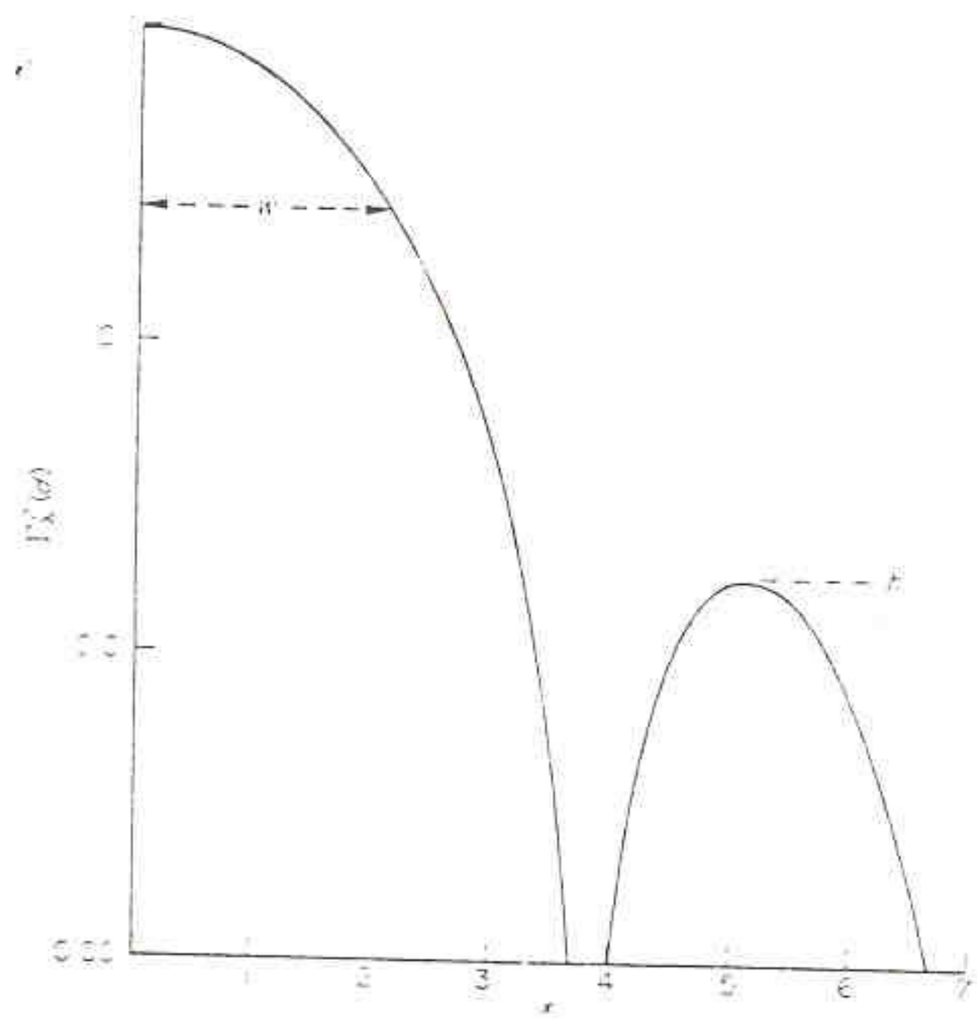

FIG. 1. *The correlation factor* $\Gamma_\lambda^2(d)$ *for a uniformly bright circular disc. The abscissa* $x = \pi\theta_{E/D}\, d/\lambda_0$; *the curve assumes no partial resolution* ($\Delta_\lambda = 1$).

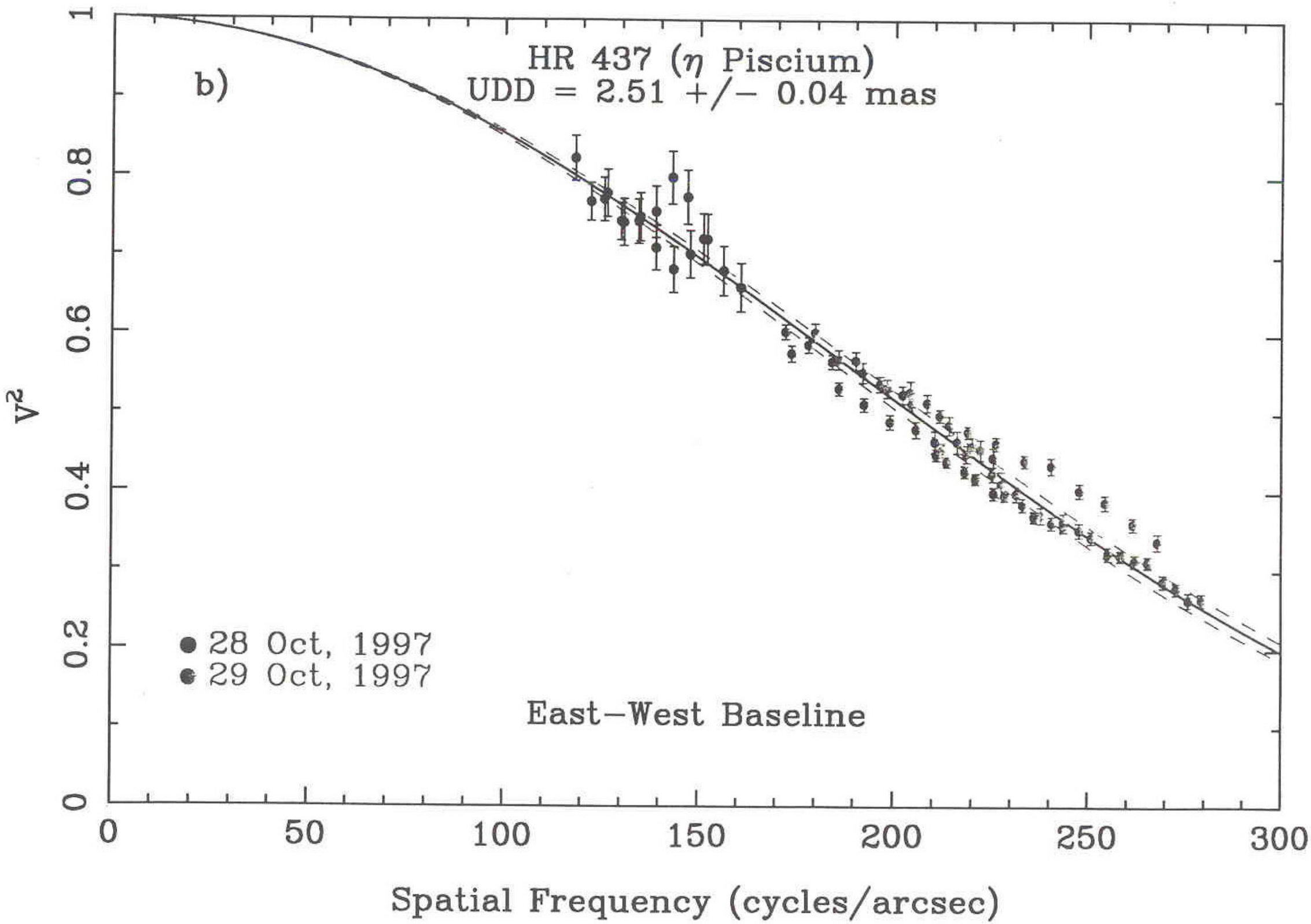
b)
HR 437 (η Piscium)
UDD = 2.51 +/− 0.04 mas
28 Oct, 1997
29 Oct, 1997
East−West Baseline
V²
Spatial Frequency (cycles/arcsec)
0
0.2
0.4
0.6
0.8
1
0
50
100
150
200
250
300

Correlation versus baseline for Sirius

Baseline (m)	Exposure (h)	Correlation Observed	Theoretical*
9·56	41·3	0·371 ± 0·007	0·377
13·07	29·4	0·160 ± 0·002	0·159
20·67	37·2	0·0107 ± 0·0015	0·0061
25·89	57·5	0·0118 ± 0·0011	0·0100
35·94	37·9	0·0001 ± 0·0013	0·0009

The uncertainty in the zero level for all observed values is ± 0·0006

* Calculated for a model atmosphere (**6**) with T_e = 10 000 K, log g = 4, λ = 4500 Å.

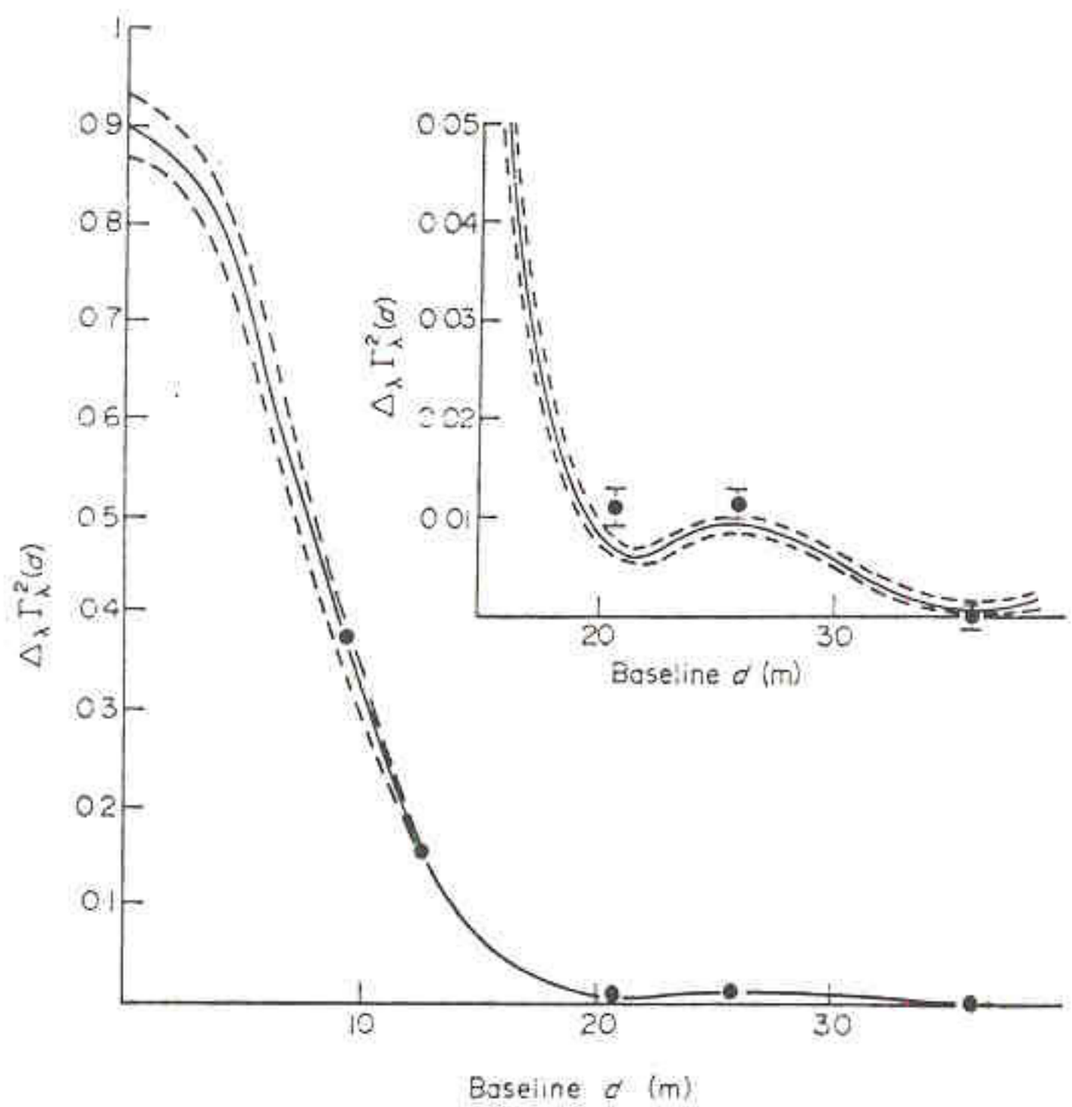

FIG. 3. *The variation of correlation $\Delta_\lambda \Gamma_\lambda$ (d) with baseline d for Sirius. The points show the observed values; the full line is a theoretical curve, based on a model stellar atmosphere (T_e = 10 000K, log g = 4), with zero-baseline correlation and angular size adjusted to give the best fit to the observations. The broken lines represent the rms uncertainty in the theoretical curves.*

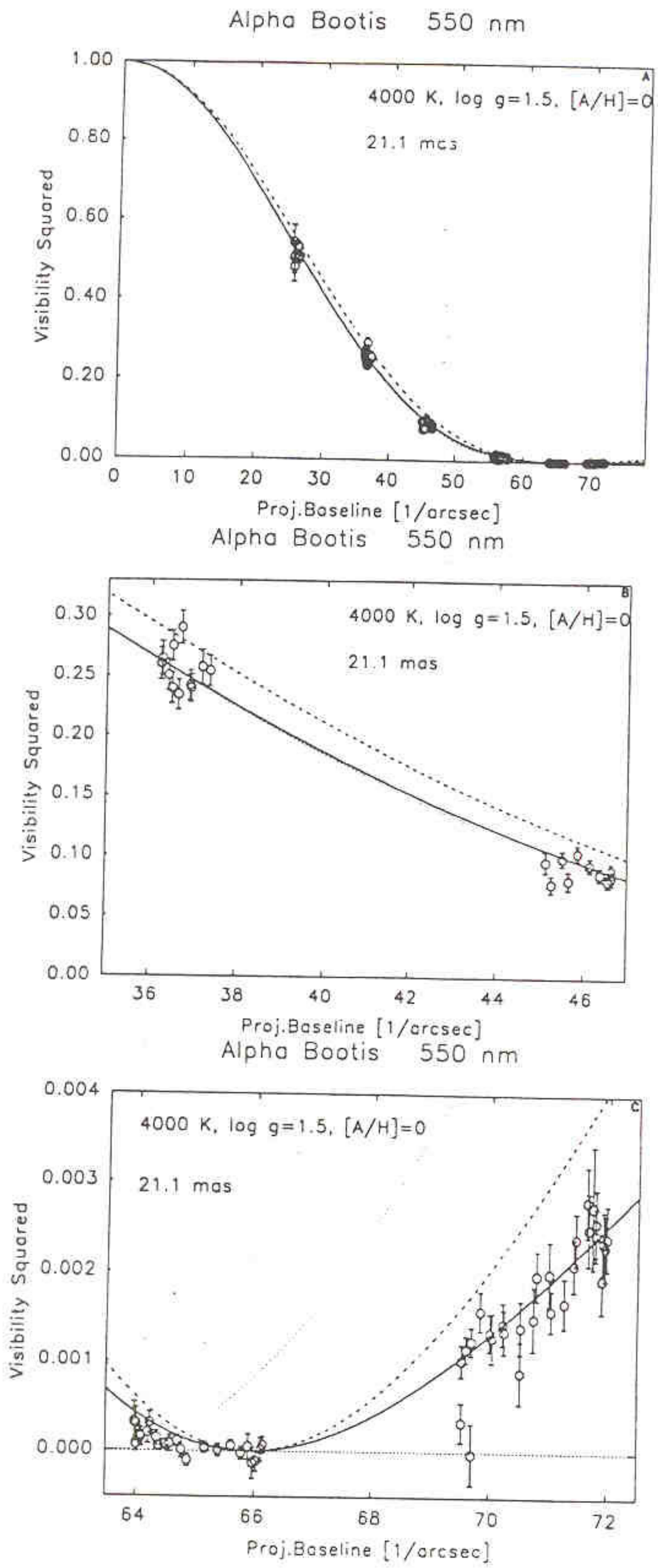

Fig. 3a–c. Visibility data at 550 nm, as a function of projected baseline length. The solid line is the prediction from the Manduca et al. model with T_{eff} = 4000 K, θ_{LD} = 21.1 mas. The dotted line is the uniform disk model which gives the best fit to the data on the short baselines (θ_{UD} = 19.18 mas). The dashed line is the uniform disk model with θ_{UD} = 18.50 mas; it has the first null at the same position as the limb-darkened model. Two subsets of the data are shown enlarged in b and c.

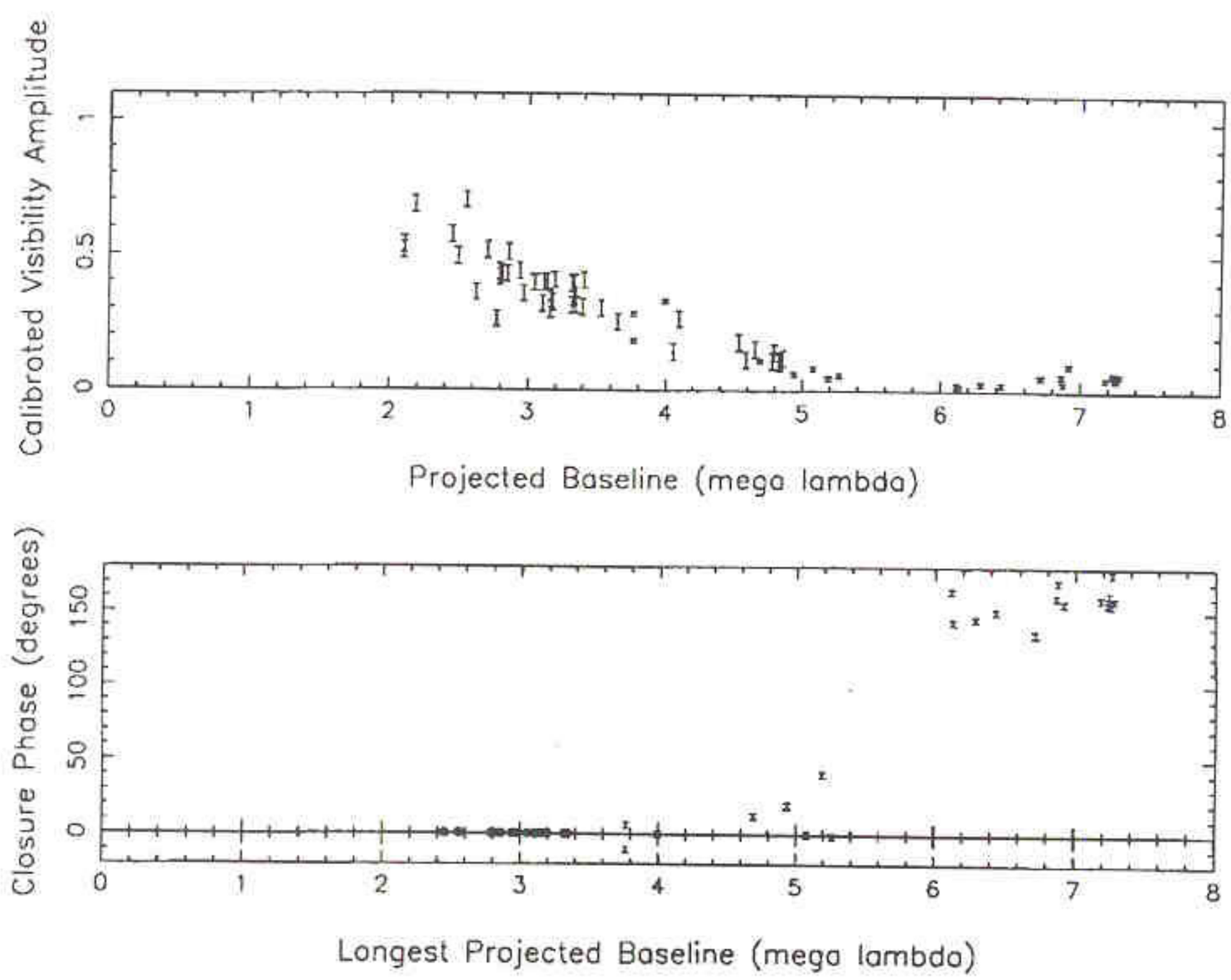

Figure 3. Calibrated visibility amplitudes (top) and closure-phases (bottom) for Betelgeuse plotted as functions of projected baseline length in wavelengths. The scatter of the measured amplitudes above visibilities of ~0.5 reflects the low source altitudes (and hence poorer and less stable seeing) at which Betelgeuse had to be observed to secure data on short baselines. For the closure-phases the projected length of the longest baseline has been used as the abscissa. Note that the value of the closure-phase flips from 0° to ~180° as the visibility amplitude reaches zero, indicating the crossing of a visibility null for a symmetric source.

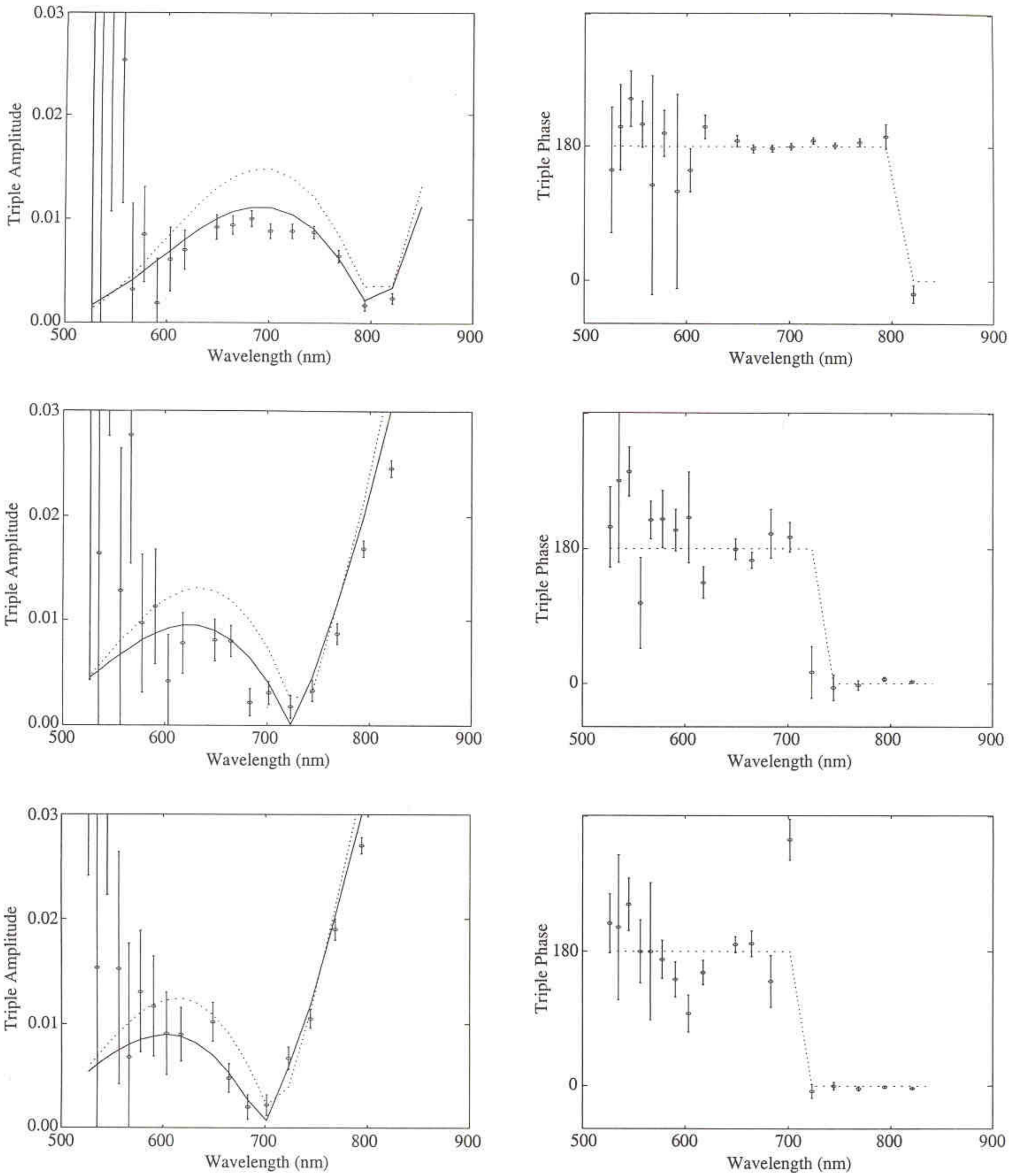
Triple Amplitude
0.03
0.02
0.01
0.00
500
600
700
800
900
Wavelength (nm)
Triple Phase
180
0
500
600
700
800
900
Wavelength (nm)
Triple Amplitude
0.03
0.02
0.01
0.00
500
600
700
800
900
Wavelength (nm)
Triple Phase
180
0
500
600
700
800
900
Wavelength (nm)
Triple Amplitude
0.03
0.02
0.01
0.00
500
600
700
800
900
Wavelength (nm)
Triple Phase
180
0
500
600
700
800
900
Wavelength (nm)

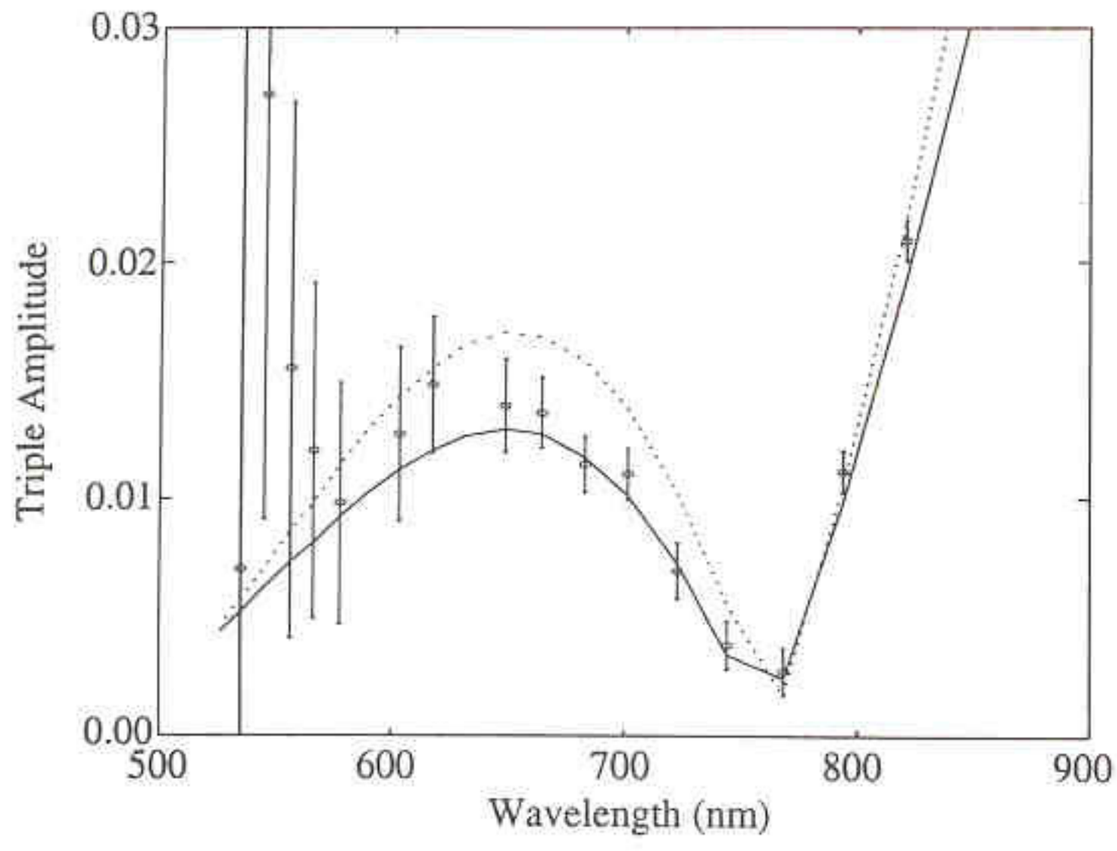
0.03
0.02
0.01
0.00
Triple Amplitude
500
600
700
800
900
Wavelength (nm)

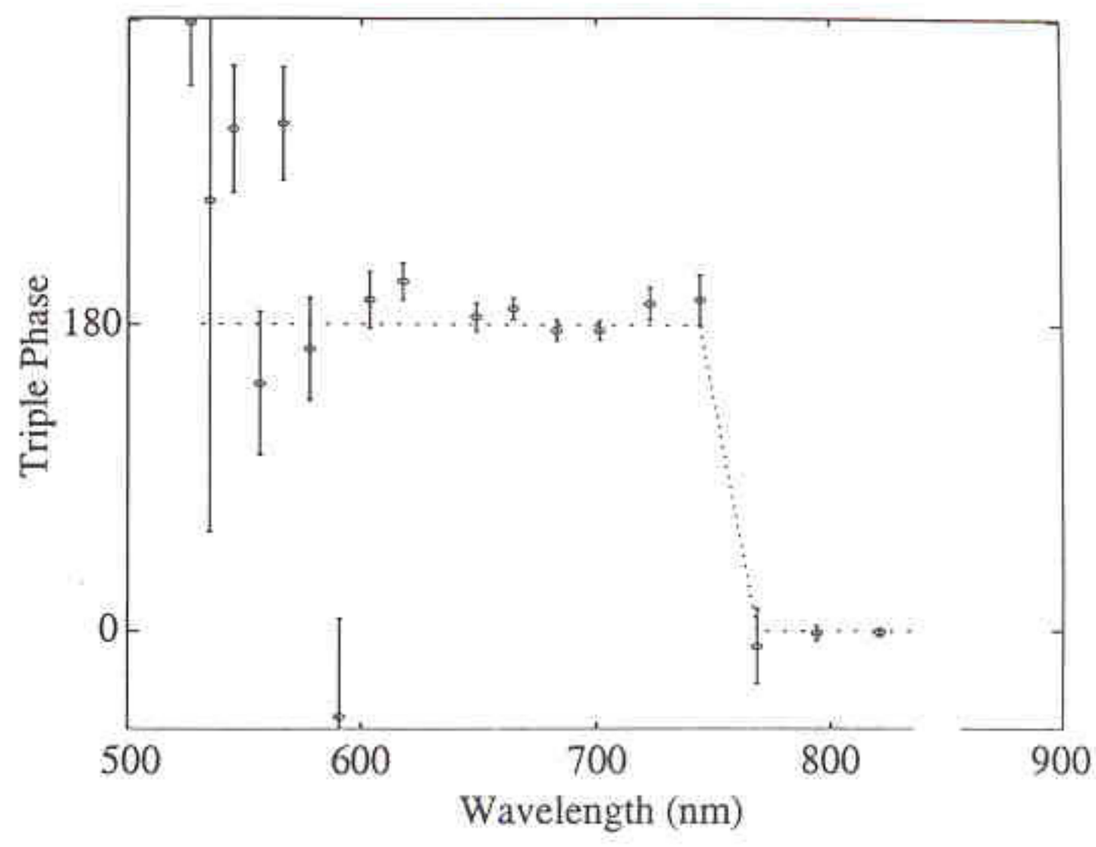
180
0
Triple Phase
500
600
700
800
900
Wavelength (nm)

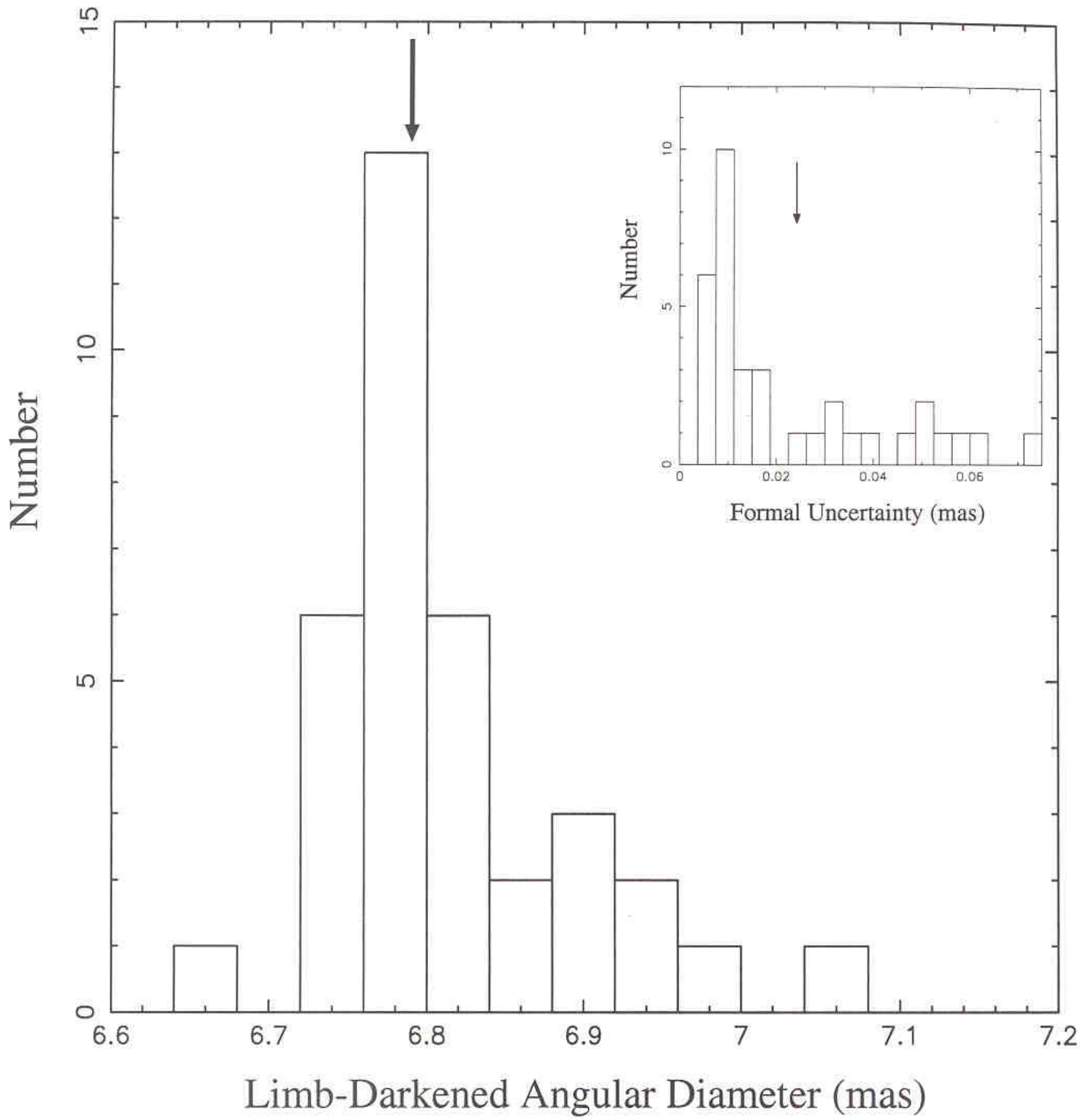
Number
15
10
5
0
6.6
6.7
6.8
6.9
7
7.1
7.2
Limb-Darkened Angular Diameter (mas)
Number
10
5
0
0
0.02
0.04
0.06
Formal Uncertainty (mas)

LIMB DARKENING

- REAL STARS ARE LIMB-DARKENED

$$I(\mu) = I_0 \left[1 - A_0 (1 - \mu) \right]$$

WHERE:

A_0 = 0th ORDER LD COEFF

$\mu = \cos \alpha$

α = ANGLE BETW. LOS & * VECTOR.

- LDDs EXIST FOR:
  - SUN (APOD 01/08/97)
  - SIRIUS (HANBURY-BROWN et al. 1974)
  - ARCTURUS (QUIRRENBACH et al. 1996)
  - α ORI (BURNS et al. 1997)
  - α CAS (HAJIAN et al. 1998)
  - α ARI

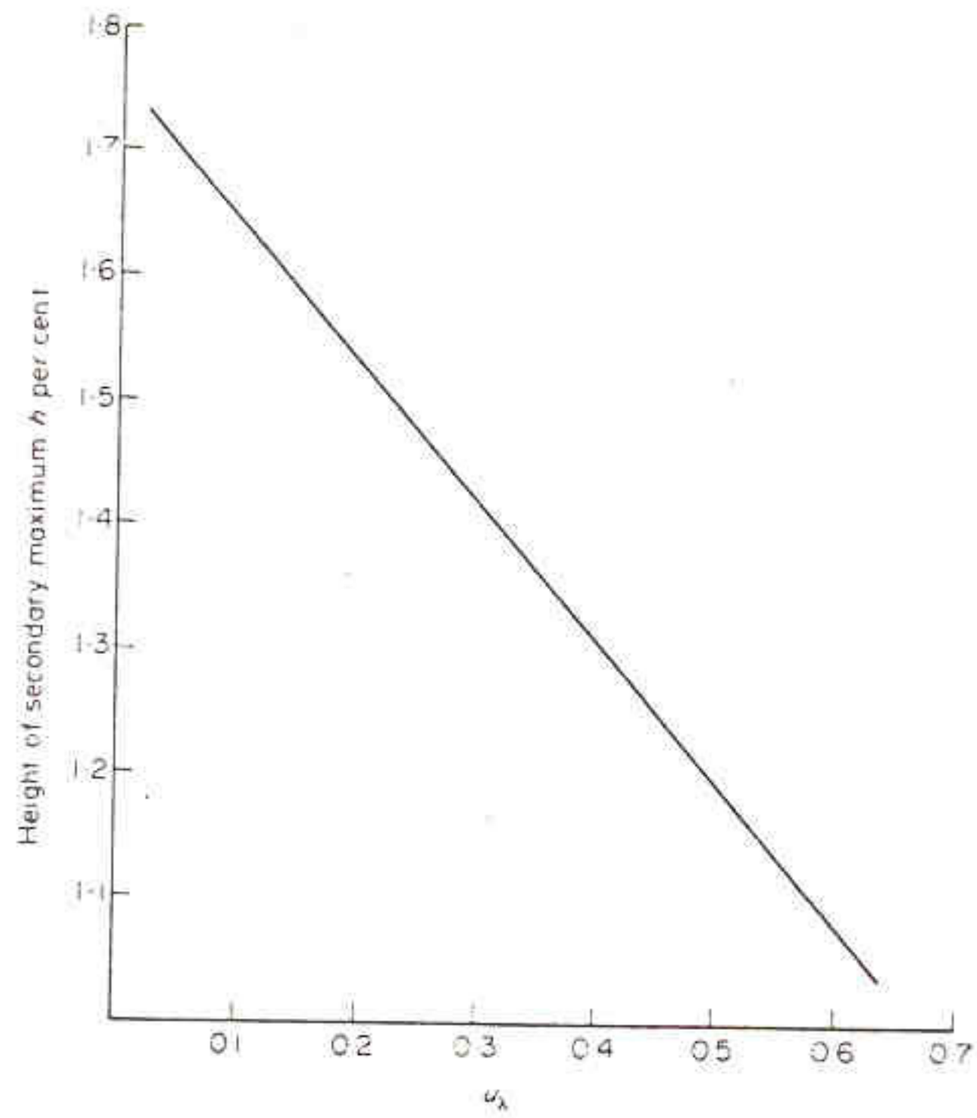

FIG. 2. *Height of secondary maximum h of correlation factor, expressed as a percentage of zero-baseline correlation (see Fig. 1) as a function of the limb-darkening coefficient* u_λ.

Uniform Disk
5.24 mas

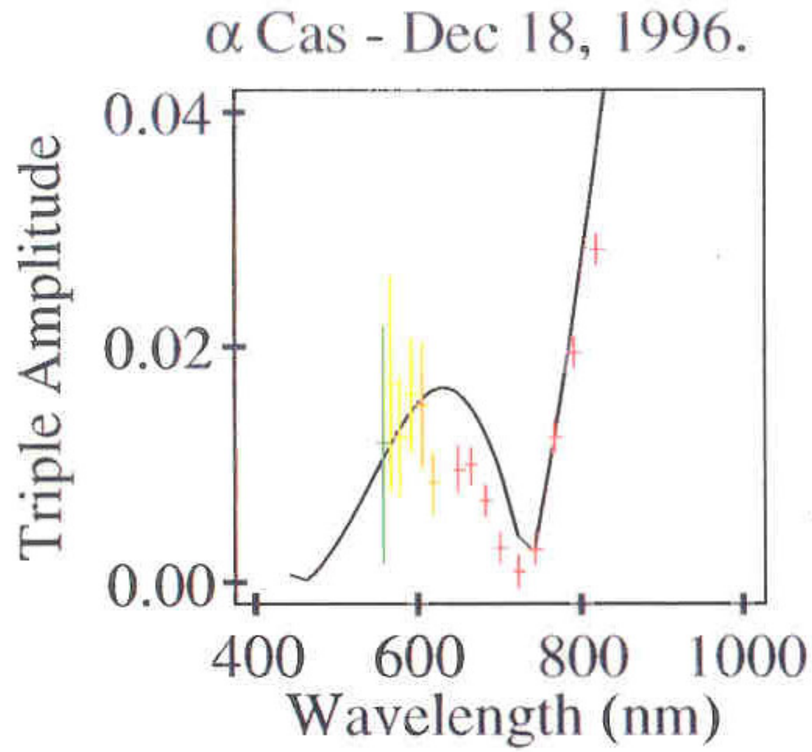
α Cas - Dec 18, 1996.
Triple Amplitude
0.04
0.02
0.00
400
600
800
1000
Wavelength (nm)

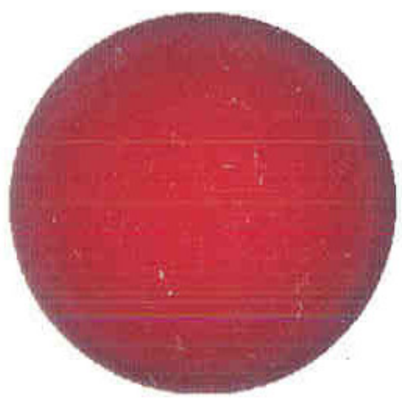
Limb-Darkened Disk
5.58 mas

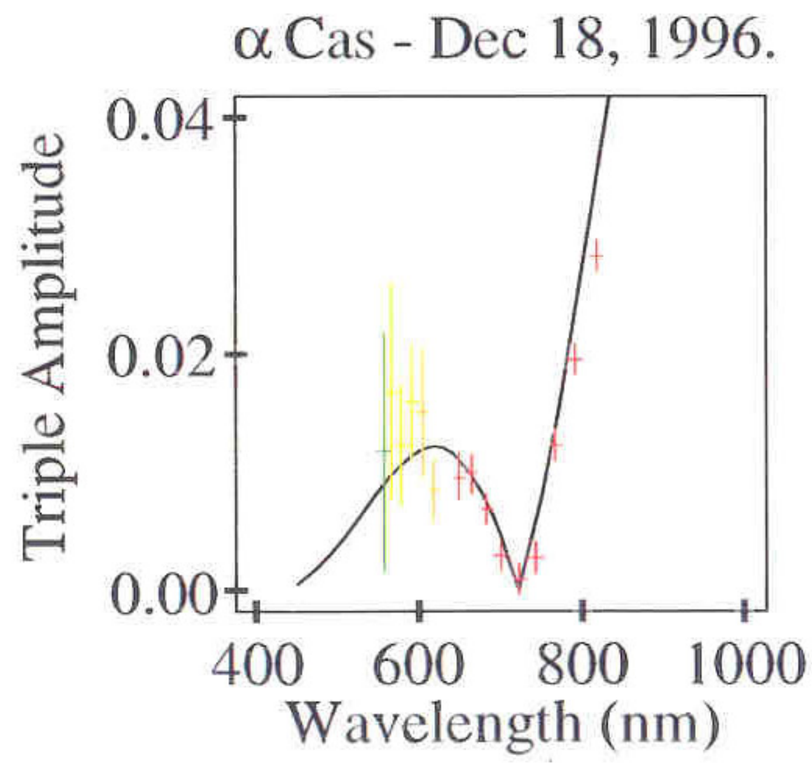
α Cas - Dec 18, 1996.
Triple Amplitude
0.04
0.02
0.00
400
600
800
1000
Wavelength (nm)

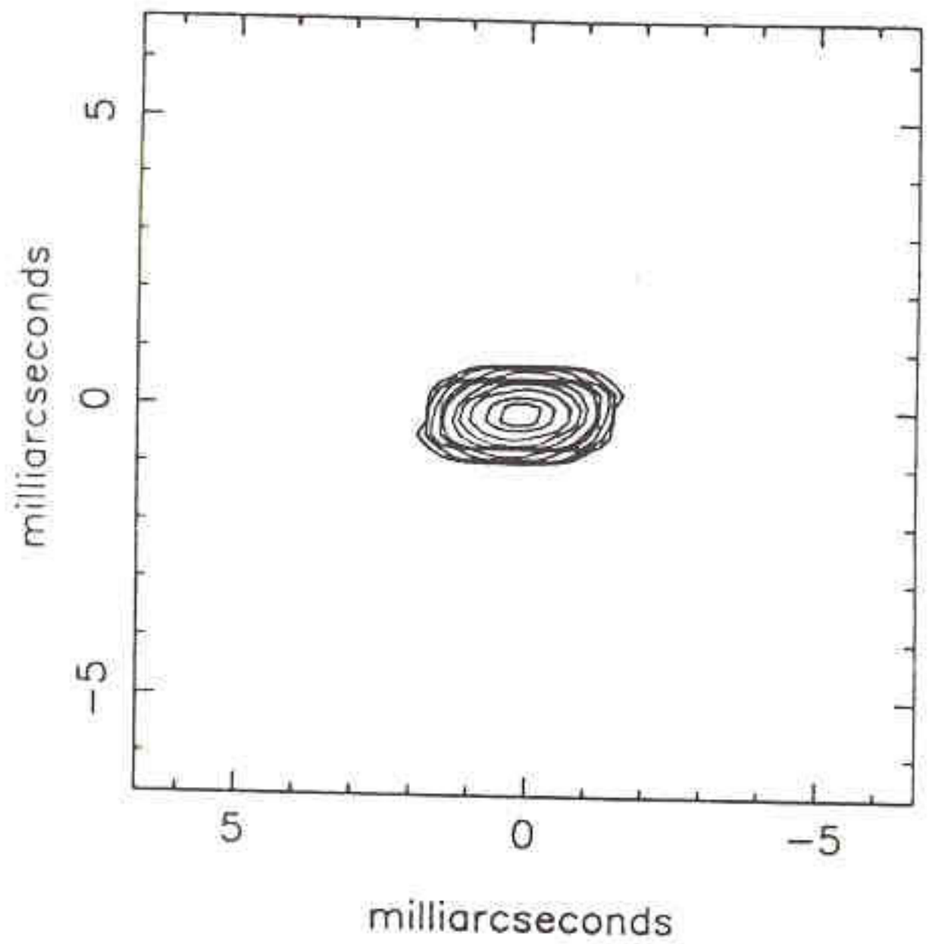

Fig. 2. Maximum-entropy reconstruction of ζ Tauri in the continuum channel centered at 550 nm. Contour levels are 0.1, 0.2, 0.5, 1, 2, 5, 10, 20, 50, and 80% of the peak.

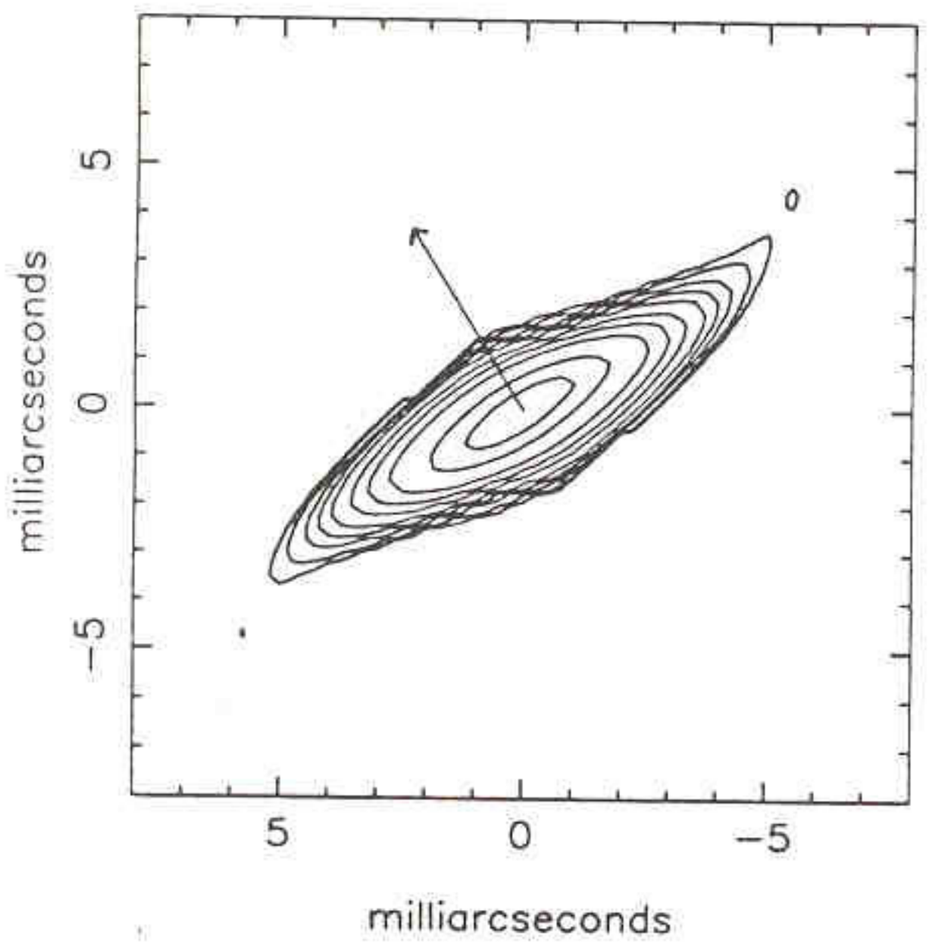

Fig. 3. Maximum-entropy reconstruction of ζ Tauri in the Hα emission line (656 nm). Contour levels are as in Fig. 2. The arrow indicates the position angle of the linear polarization.

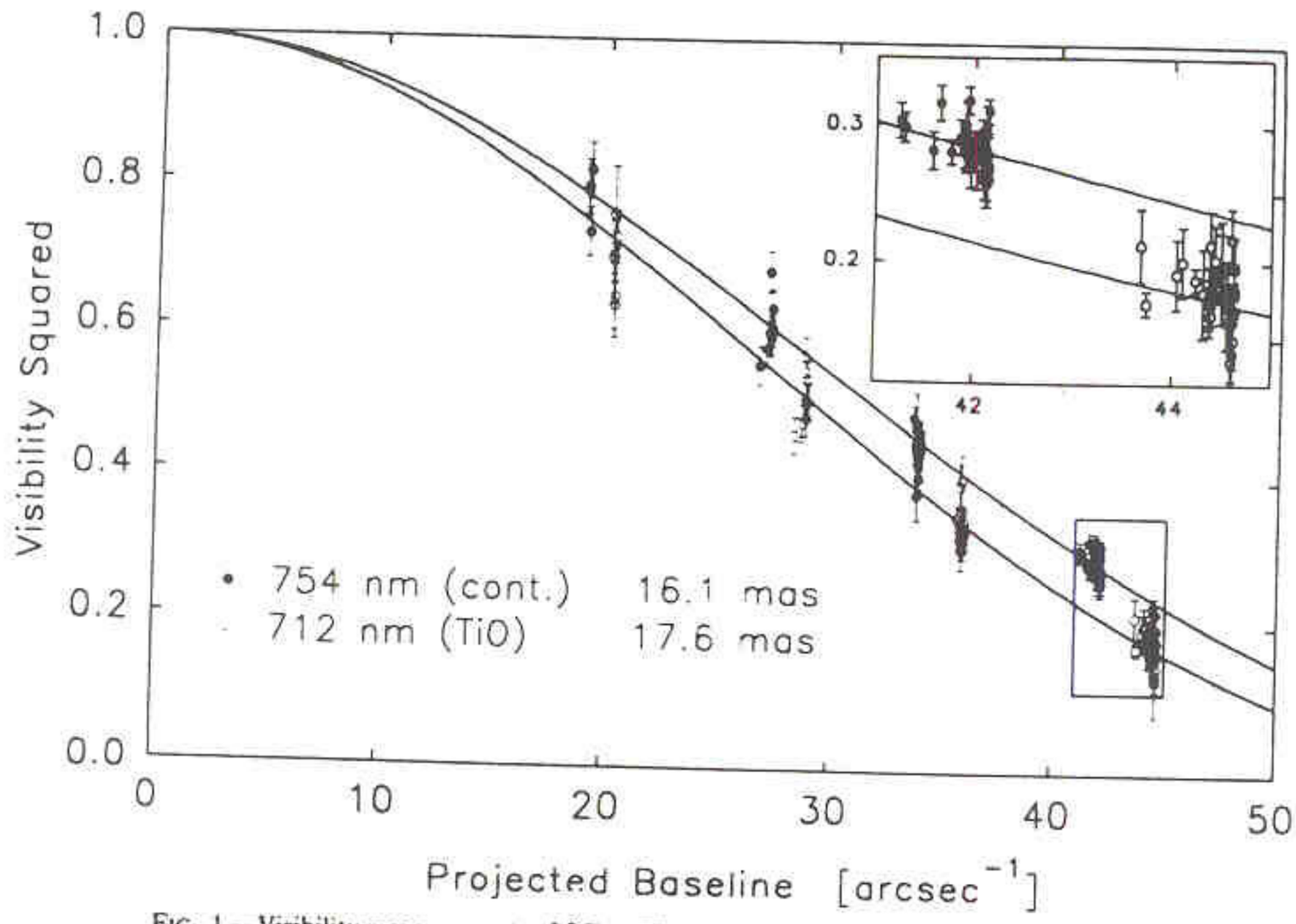

FIG. 1.—Visibility measurements of β Peg. The data points represent individual scans of 75 s.

SUMMARY OF RESULTS[a]

Star	BS	Spectral Type	$R-I$	UDD at 712 nm (mas)	UDD at 754 nm (mas)	Diameter Ratio
β And	337	M0 IIIa	1.00	12.73 ± 0.18	12.63 ± 0.22	1.01 ± 0.02
α Cet	911	M1.5 IIIa	1.00	11.95 ± 0.23	11.66 ± 0.22	1.02 ± 0.03
ρ Per	921	M4 II	1.62	16.03 ± 0.29	14.66 ± 0.20	1.09 ± 0.02
α Tau	1457	K5 III	0.94	19.88 ± 0.14	19.80 ± 0.12	1.00 ± 0.01
119 Tau	1845	M2 Iab–Ib	1.44	11.47 ± 0.33	9.98 ± 0.20	1.15 ± 0.04
π Aur	2091	M3 II	1.31	8.90 ± 0.29	8.23 ± 0.21	1.08 ± 0.04
η Gem	2216	M3 III	1.31	11.75 ± 0.27	10.70 ± 0.15	1.10 ± 0.03
μ Gem	2286	M3 IIIab	1.38	13.97 ± 0.28	13.50 ± 0.13	1.03 ± 0.02
δ Lyr	7139	M4 II	1.63	11.76 ± 0.30	10.85 ± 0.26	1.08 ± 0.04
R Lyr	7157	M5 III	1.91	18.66 ± 0.31	16.64 ± 0.25	1.12 ± 0.02
μ Cep	8316	M2 Iae	1.76	25.03 ± 0.43	21.31 ± 0.28	1.17 ± 0.02
β Peg	8775	M2.5 II–III	1.32	17.55 ± 0.14	16.11 ± 0.11	1.09 ± 0.01

[a] For each star, the table lists the Bright Star number, spectral type, $R-I$ color index, uniform disk diameters at 712 and 754 nm, and the ratio of these diameters.

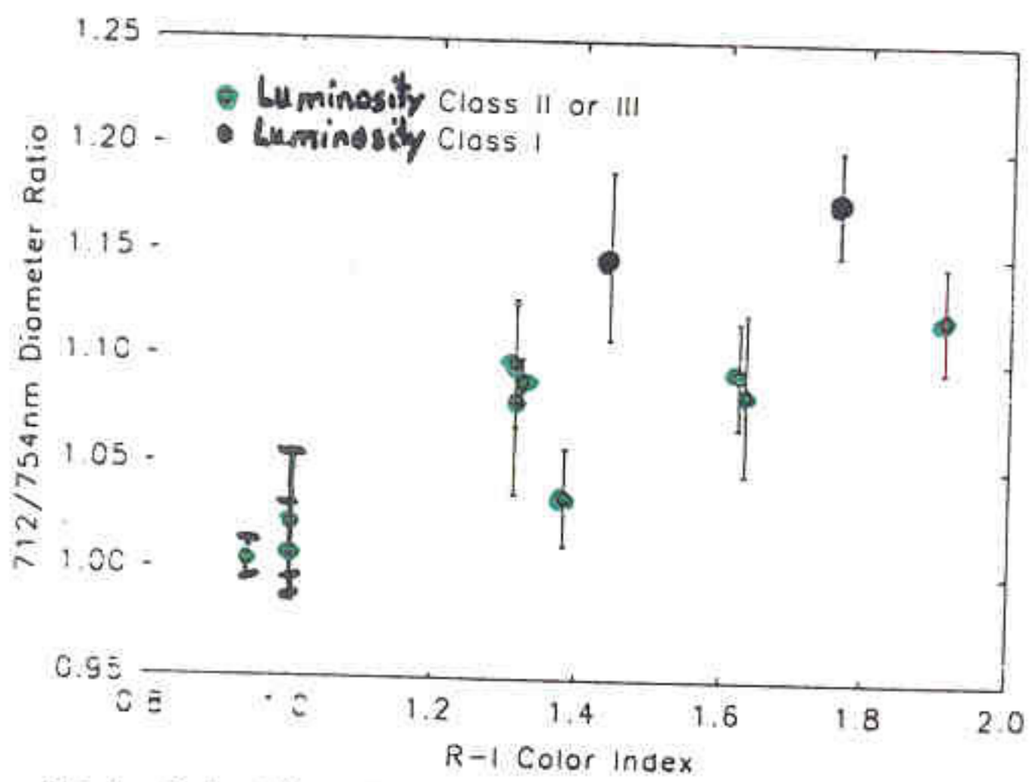

FIG. 2—Ratio of the uniform disk diameters measured at 712 and 754 nm as a function of $R-I$ color index.

NON-CIRCULAR STARS

- MANY STARS ARE STRONGLY ELONGATED

- Be, LATE GIANTS, PPNe, PNe,

aries.usno.navy.mil/ad/pne

- GENERALLY NEED SPECTRAL CHANNELS

BOOTSTRAPPING

- SINGLE BASELINE HAS PROBLEMS FOR $V^2 < 0.01$

- USE λ AND/OR ϕ BOOTSTRAPPING

- λ BOOTSTAPPING
  - TRACK ON LONG λ
  - RECORD SIMULTANEOUSLY ON SHORT λ
  - NEED BIG $\Delta\lambda$ $\rightarrow$ VACUUM PATHS

- ϕ BOOTSTRAPPING
  - PHASE UP SHORT BASELINES
  - LONG BASELINE(S) MAY BE OK!
  - BEST FOR LINEAR ARRAY

SPOTS

- STARS (i.e. SUN) HAVE SPOTS
- DOPPLER IMAGING
  - SPECTRA @ VARIOUS P.A.S
  - V_{ROT}
  - V_{TURB}
  - i
- RESULTS CAN BE AMBIGUOUS!
  - $V_{RAD}(t)$
  - $W(t)$
  - $\Delta V(t)$

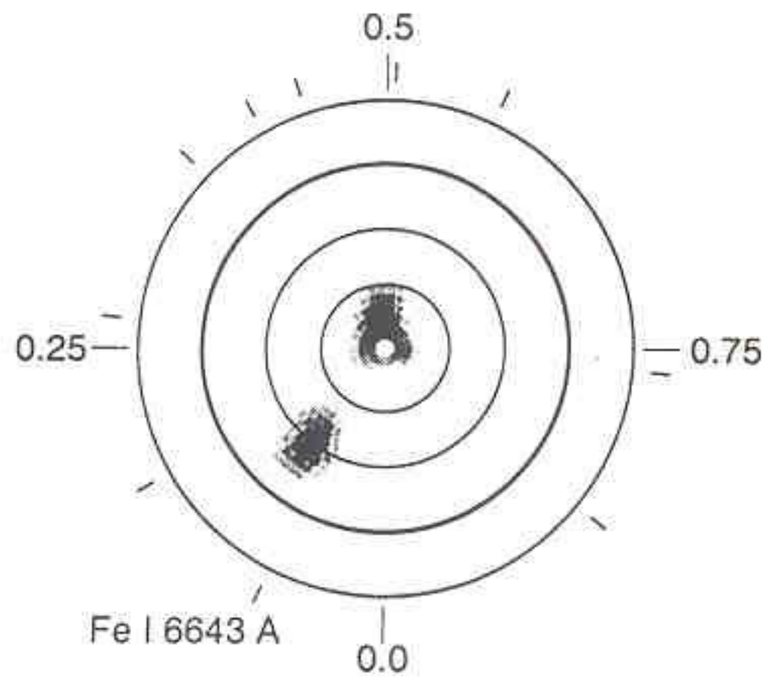

Fig. 4. The Doppler image derived using the Fe I 6643 Å line. Darkest regions are 650 K below the photospheric temperature.

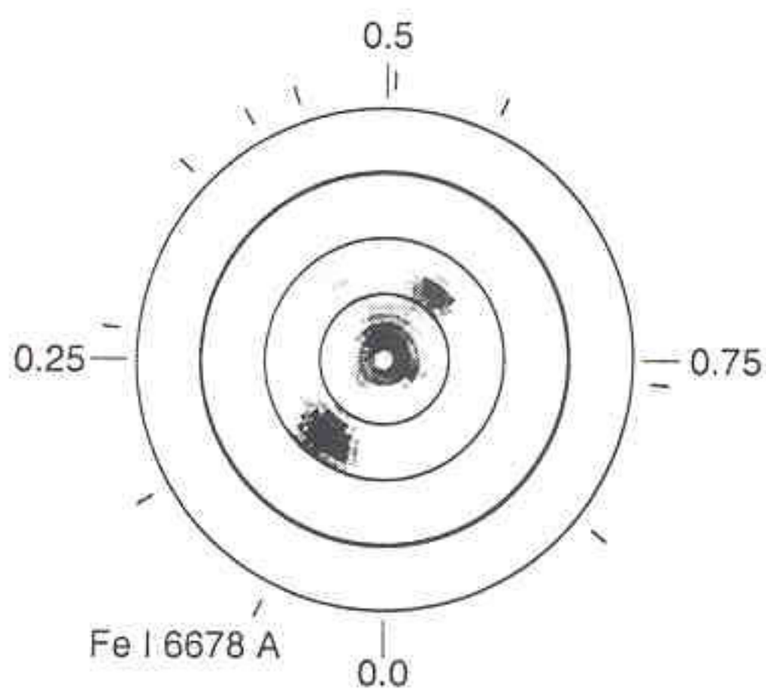

Fig. 5. Doppler image derived using Fe I 6678 Å. Darkest regions are 870 K below the photospheric temperature.

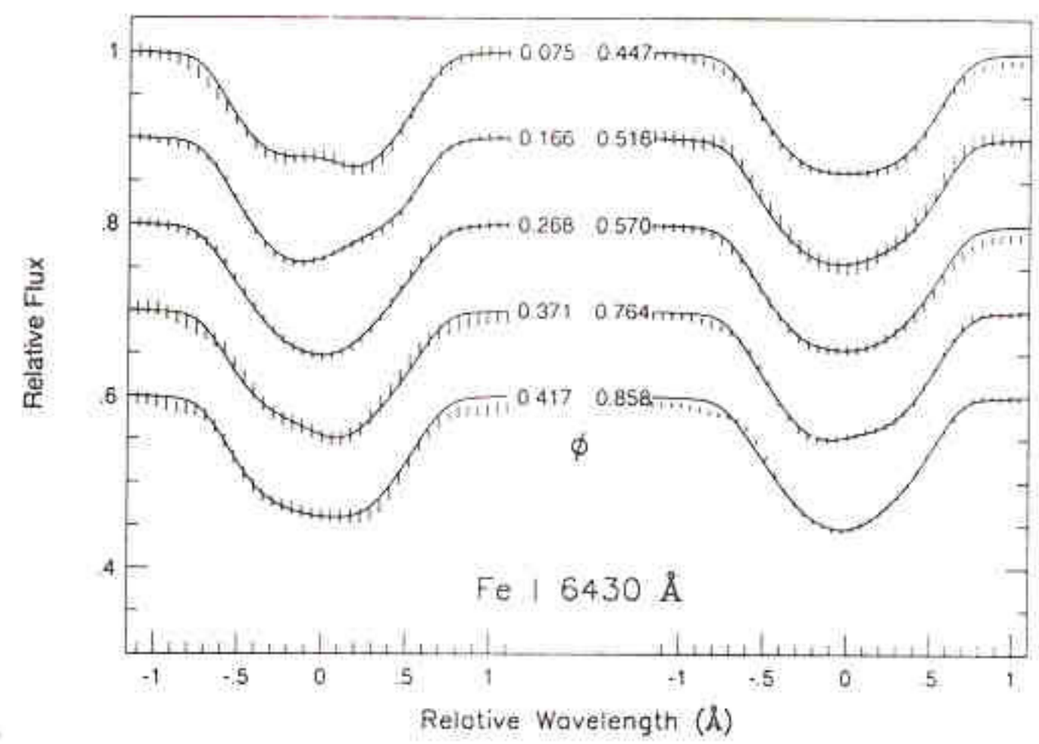

Fig. 6. The observed spectral line profiles (vertical bars) for Fe I 6430 Å and the predicted profiles (lines) from the Doppler image. The length of each vertical bar is an indication of the error in the flux measurement.

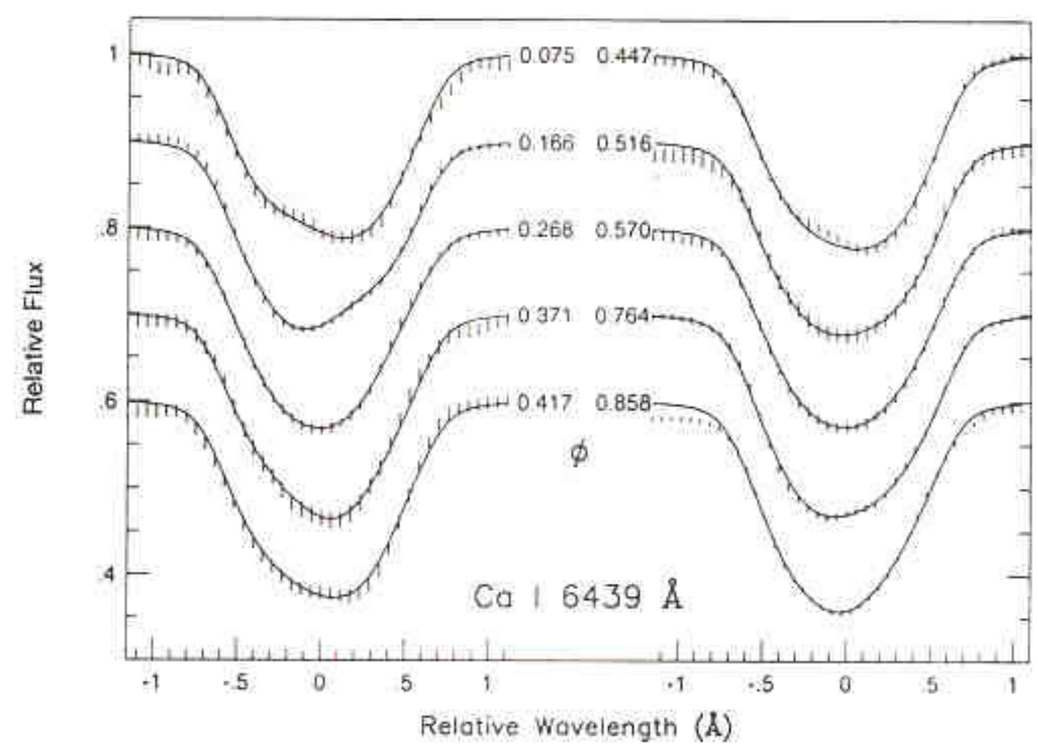

Fig. 7. The observed spectral line profiles (vertical bars) for Ca I 6439 Å and the predicted profiles (lines) from the Doppler image used in the reconstruction

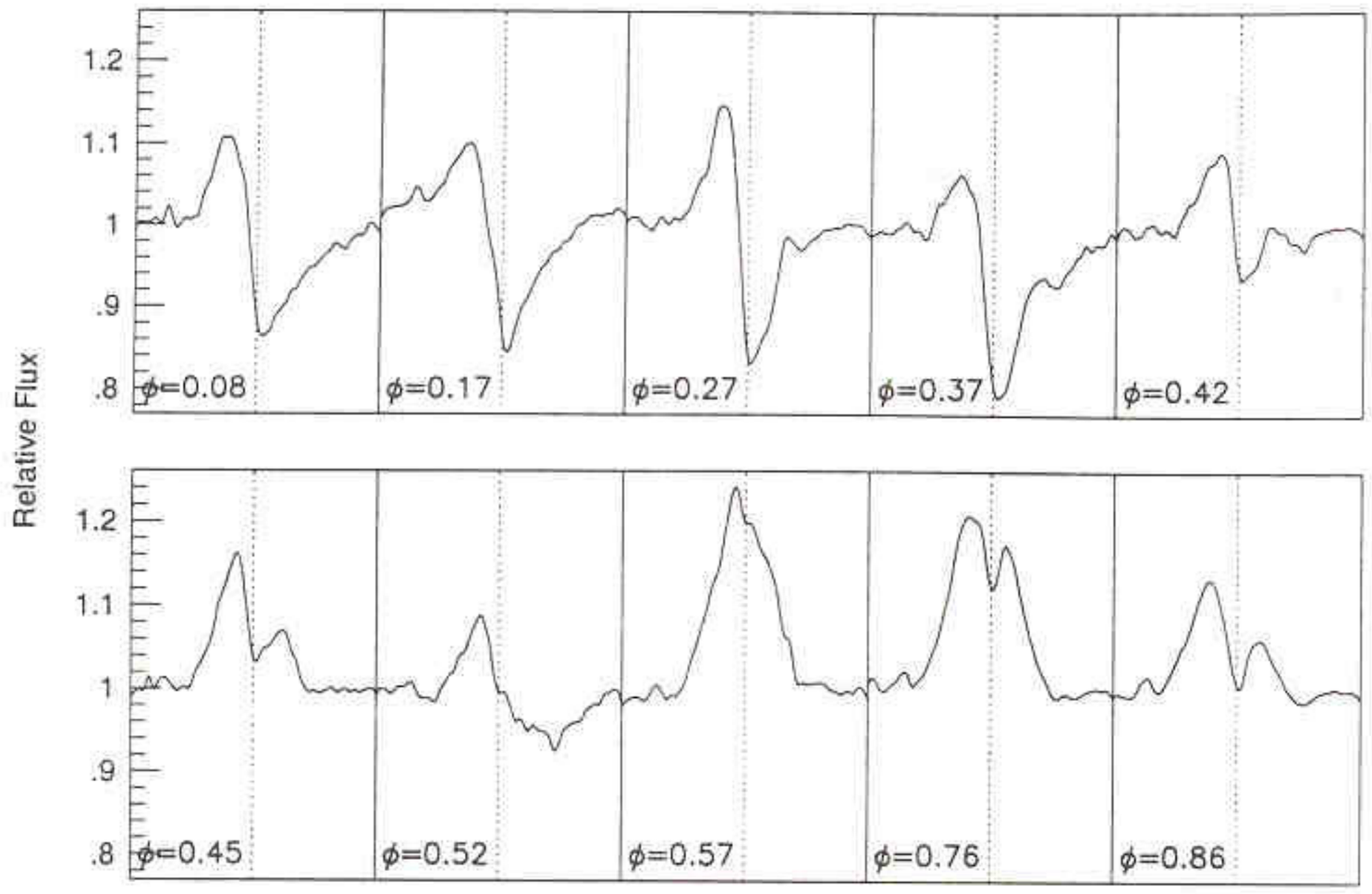

Fig. 9. Observed Hα line profiles as a function of orbital phase. The dashed line represents the center of Hα as measured with respect to the photospheric lines.

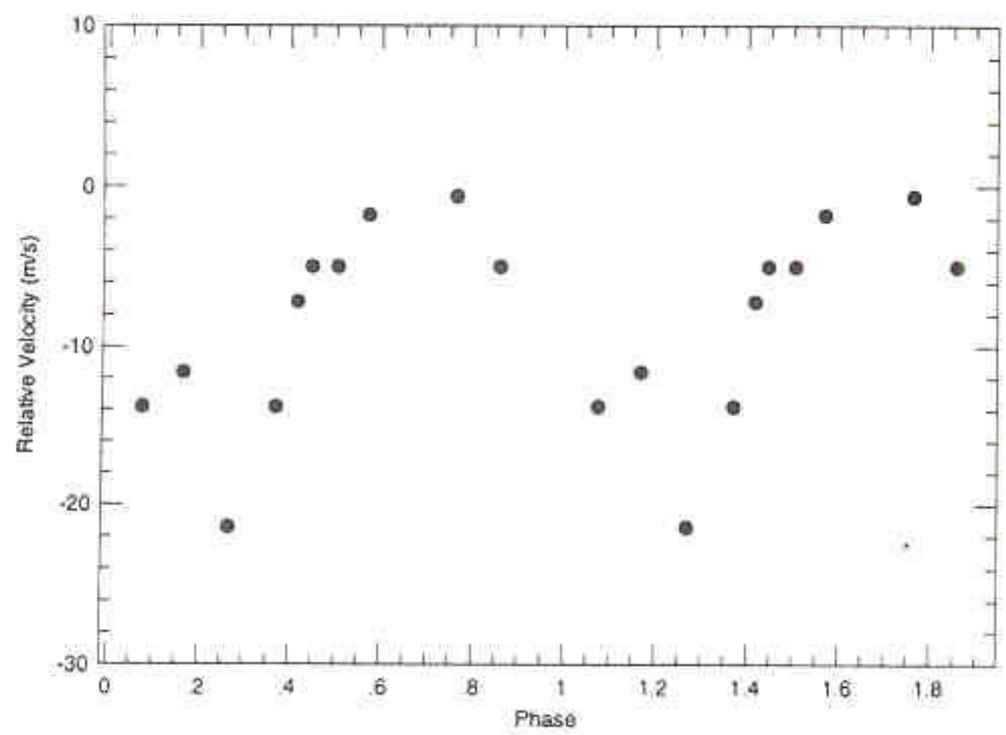

Fig. 10. The radial velocity variation of the Hα emission profile after subtracting underlying absorption profile. Points are repeated for the second cycle.

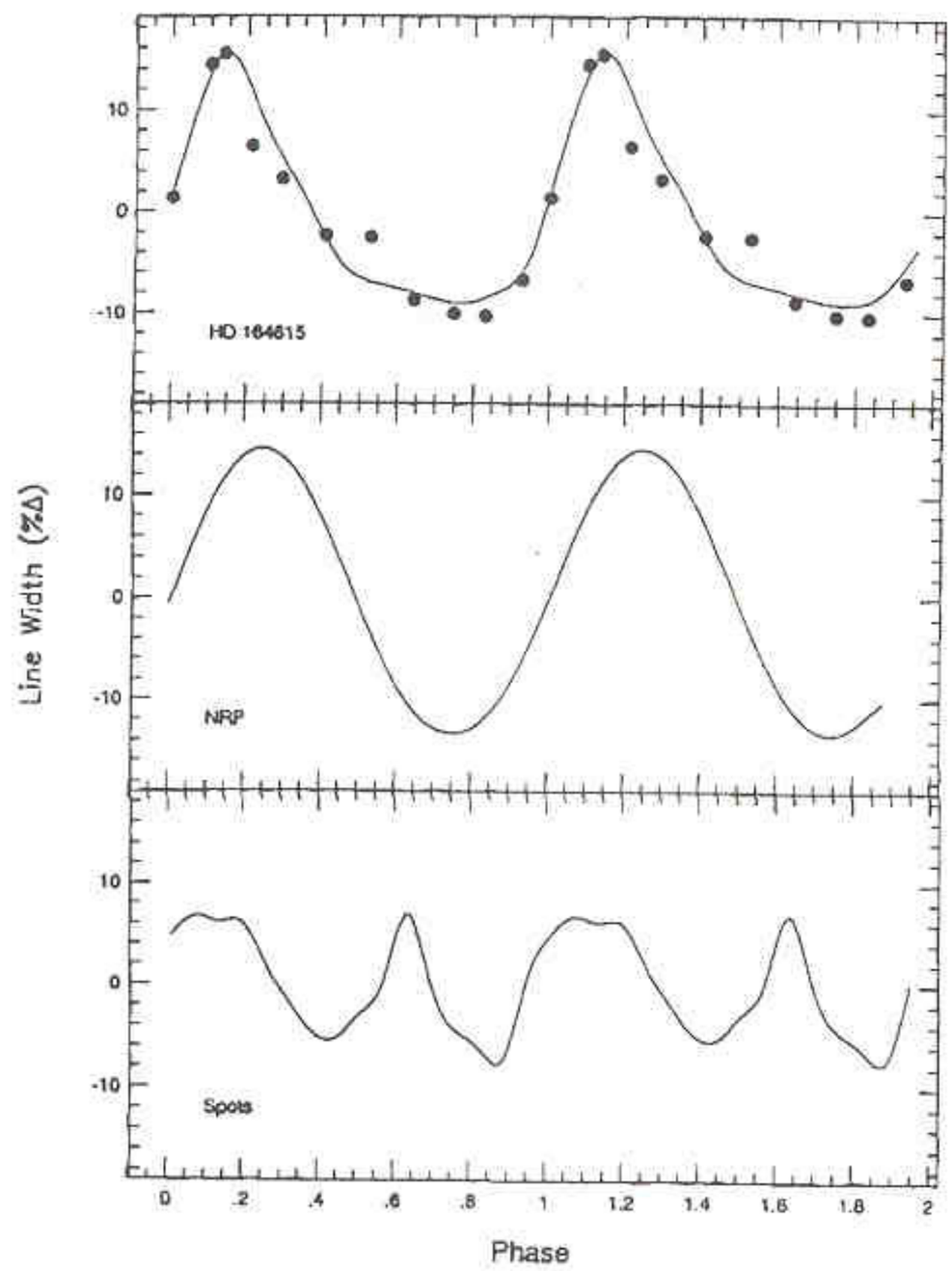

Figure 7. (Bottom) The predicted linewidth varations from the spot model. (Middle) The predicted linewidth variations from an $m = 2$ pulsation mode with a constant pulsation amplitude of 6.5 km s^{-1}. (Top) The points represent the observed linewidth variations of Fe II 5318 Å. The line represents the predicted linewidth variation for an $m = 2$ mode that has a pulsational amplitude as a function of phase as shown in Fig. 2.

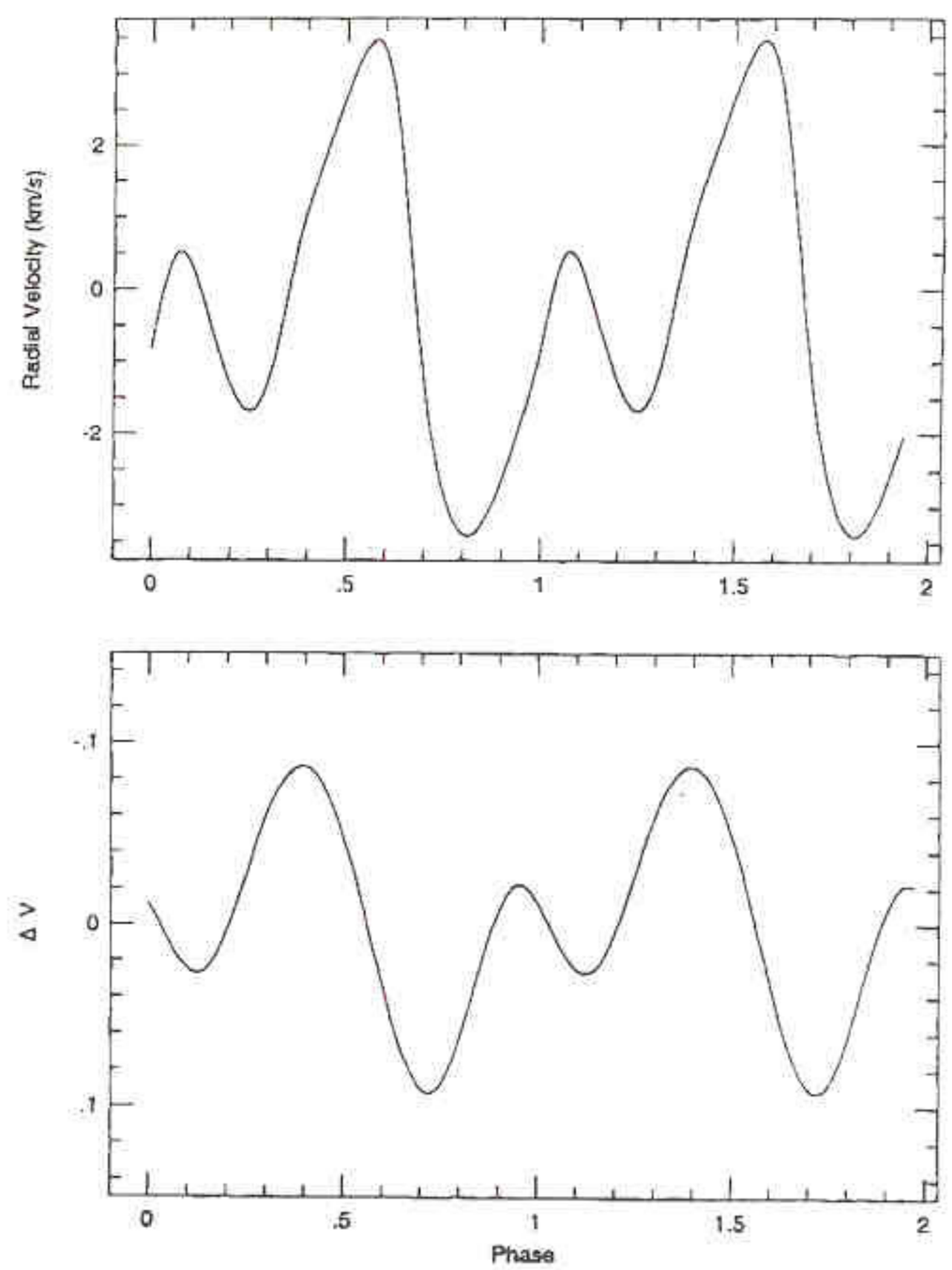

Figure 8. (Top) The predicted radial velocity variations from the spot model. (Bottom) The predicted photometric variations from the spot model.

High-resolution spectral observations have been presented for HD 164615 which show systematic changes in the line profile shapes with the photometric period. These changes along with the RV variations are best fitted with an $m = 2$ non-radial mode. A star-spot model can provide reasonable fits to the line profile variations, but it is incapable of fitting the changes in the linewidths or the observed RV curve. Furthermore, the spot model has a predicted photometric amplitude at least 5 times that which is observed for this star. Finally, the derived 'Doppler image' for HD 164615 is consistent with that produced by non-radial pulsations. All of these establish that non-radial pulsations are indeed responsible for the light variations in HD 164615 and that this star, along with the other 'γ Dor' variables, represents a new class of pulsating stars.

~~SPECKLE~~ APERTURE MASKING

- PUT MASK WITH HOLES ON SCOPE

- SIMULATES PHASED, MULTI-ELEMENT OPTICAL ARRAY

- LIMITED BASELINES

- USE OF CLOSURE PHASES $f = 1 - \frac{2}{N}$

- GREAT!!! IMAGES

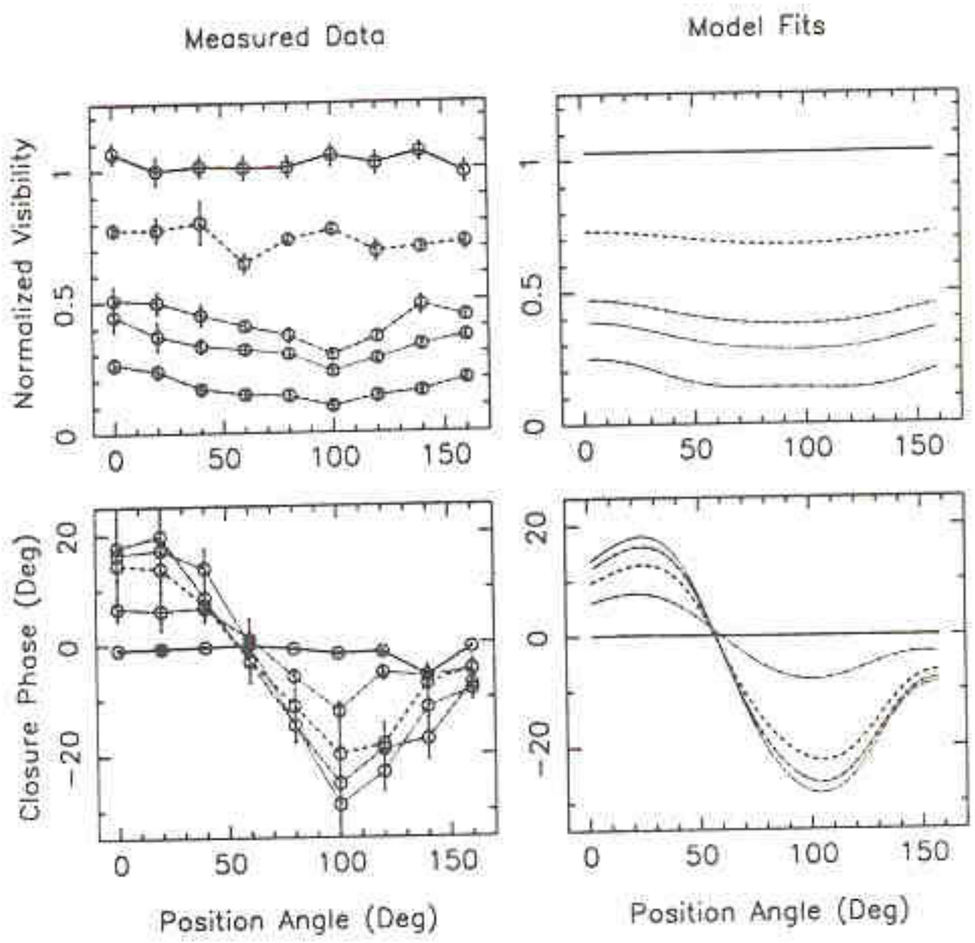

Figure 3. Calibrated visibility amplitudes and closure phases as obtained for α Her at 633 nm in 1993 June. The left-hand panels show the measured data, and the right-hand panels the fits for a model composed of a uniform disc together with two unresolved hotspots on the stellar surface. For clarity, only data corresponding to 5 of the interferometer baselines and 5 of the closure triangles are shown. In these, and subsequent plots, lower azimuthally averaged visibilities correspond to longer interferometer baselines. One-sigma error bars are plotted. For a symmetric source all the closure phases should be zero.

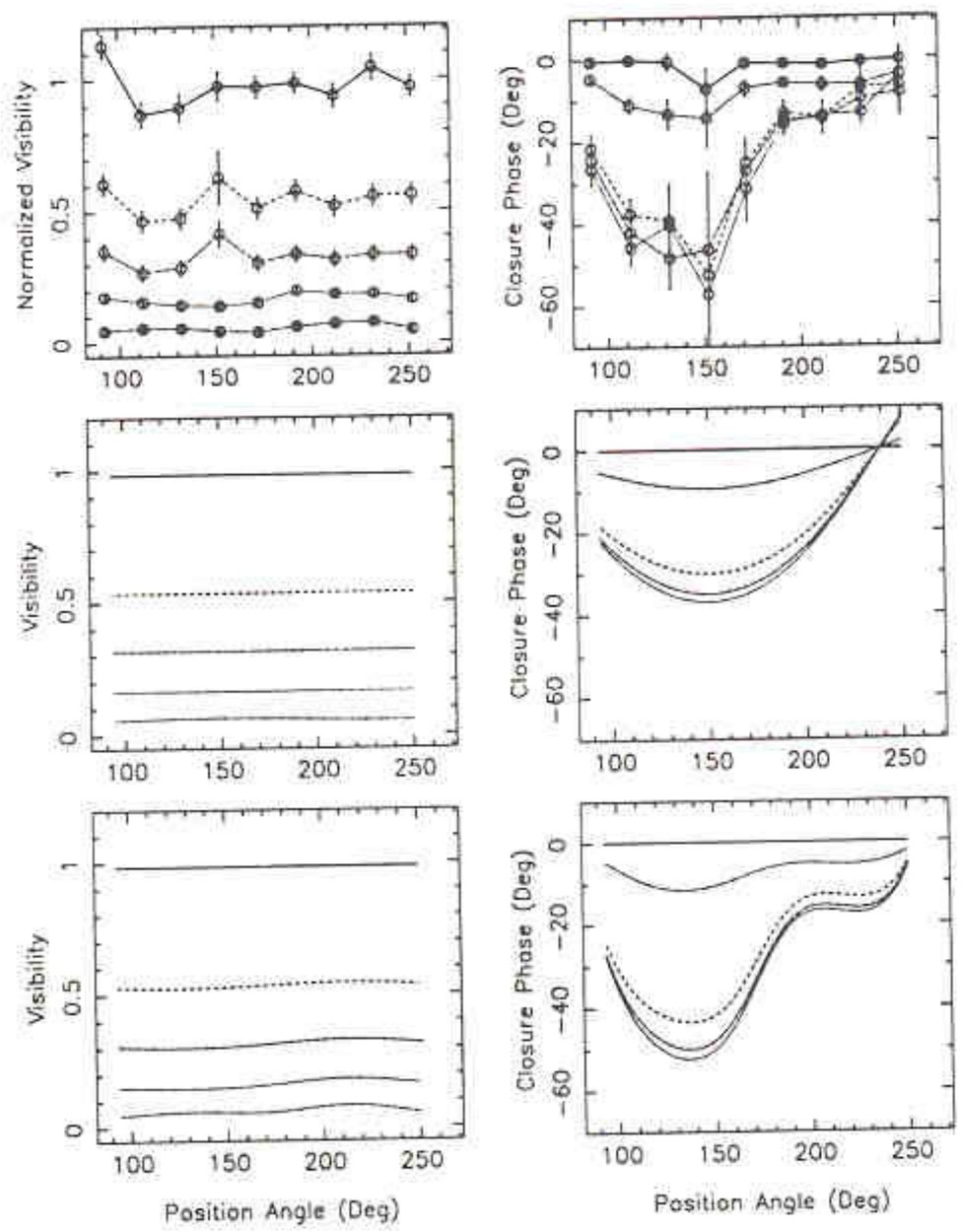

Figure 4. Calibrated visibility amplitudes and closure phases as obtained for α Ori at 700 nm in 1993 December. As in Fig. 3, only data corresponding to 5 of the interferometer baselines and 5 of the closure triangles have been plotted, together with one-sigma error bars. The upper panels show the measured data, while the lower panels show the fits for two different models. The central graphs correspond to the best-fitting uniform-disc plus single spot model, while the lower plots correspond to a model comprising a uniform disc together with two unresolved hotspots.

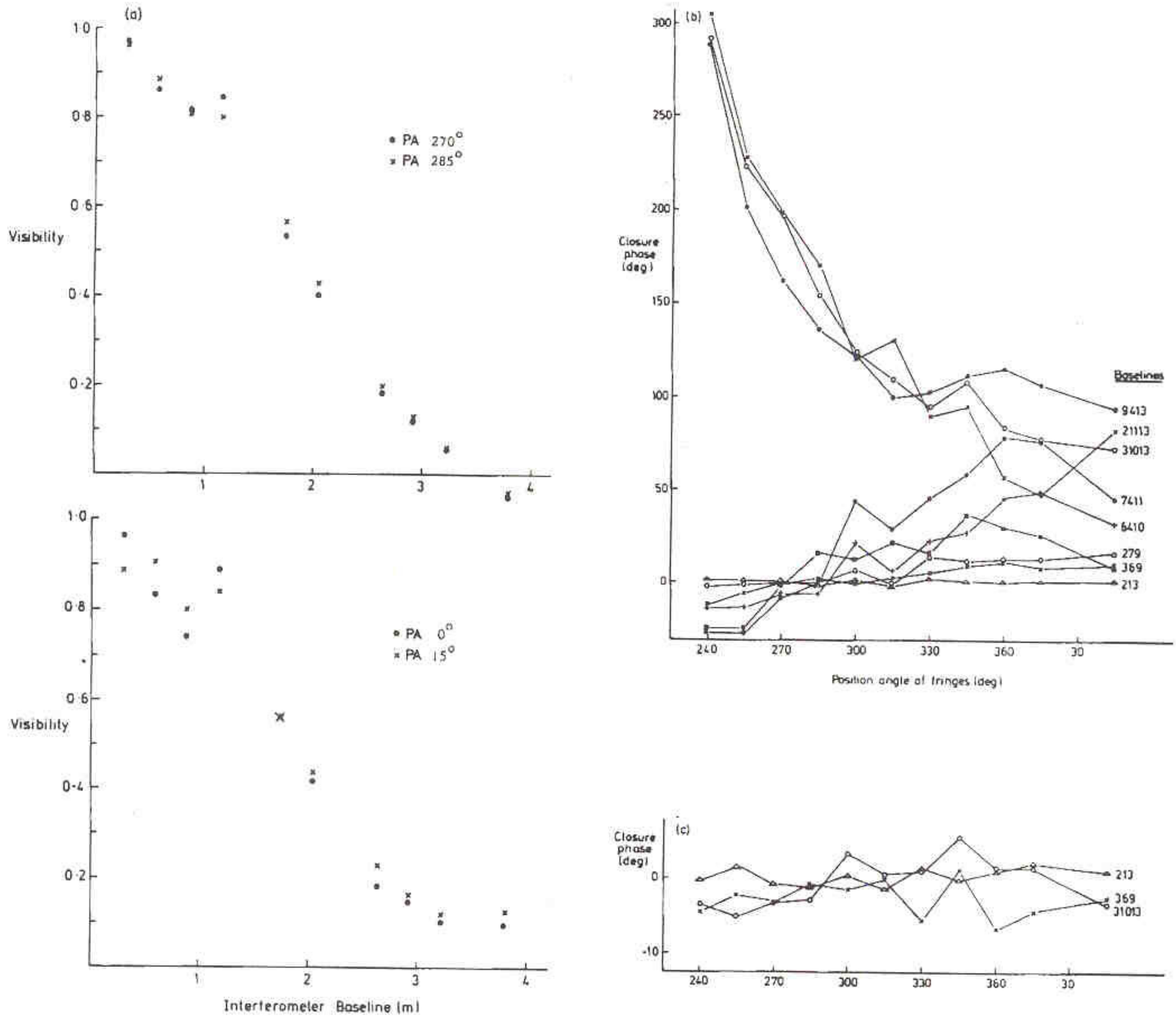

Figure 1. Calibrated visibility amplitude and closure phase data for the 710-nm, 3.8-m maximum baseline observation. This five-hole mask produces baselines of 1, 2, 3, 4, 6, 7, 9, 10, 11, 13 times 29 cm. In (a) the amplitudes are shown as a function of baseline for four position angles of the mask, while in (b) and (c) the closure phases are plotted as a function of position angle. The closure phases are labelled by concatenating the indices of the three contributing baselines. Graph (b) shows the closure phases measured for Betelgeuse, while graph (c) shows those measured for the calibration point source γ Ori. Note the change of vertical scale between (b) and (c). Only a subset of the closure phases are plotted in (c), for clarity.

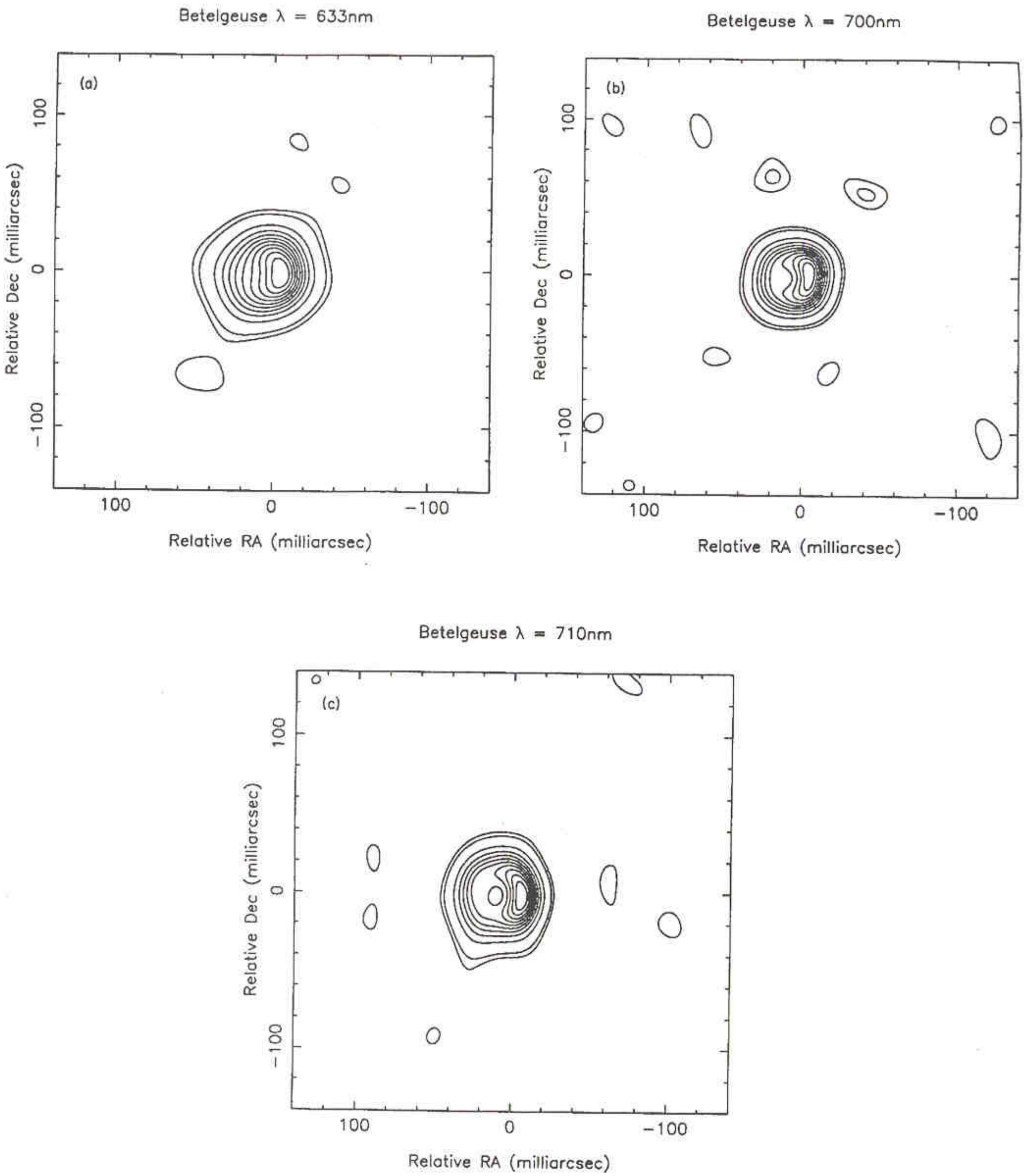

Figure 2. Reconstructed images of Betelgeuse at wavelengths of (a) 633 nm, (b) 700 nm and (c) 710 nm, with resolutions of 48, 38 and 39 mas, respectively. The contour levels are at 1, 2, 10, 20, 30,... 80, 90 per cent of the peak brightness. The images show a moderate amount of 'super-resolution', because the maximum entropy algorithm used to reconstruct them allows *a priori* constraints, such as positivity and finite extent of the image, to be enforced. The spots outside the central disc are consistent with the expected noise level.

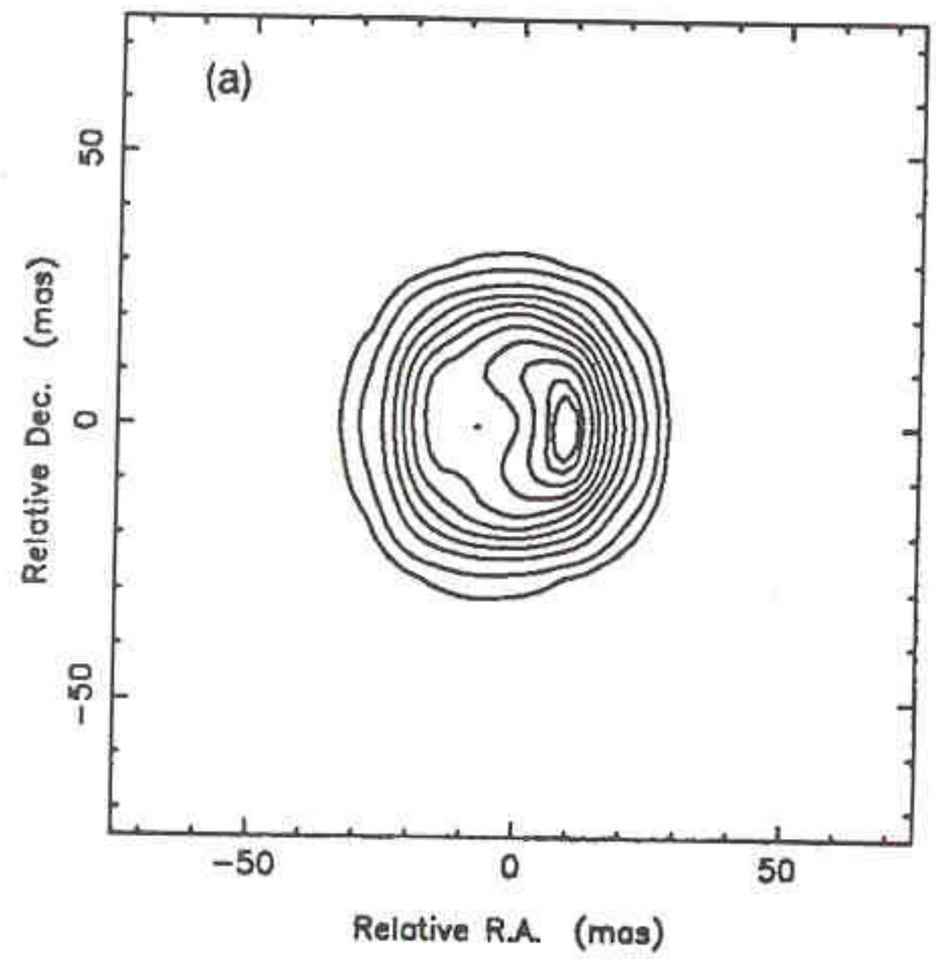

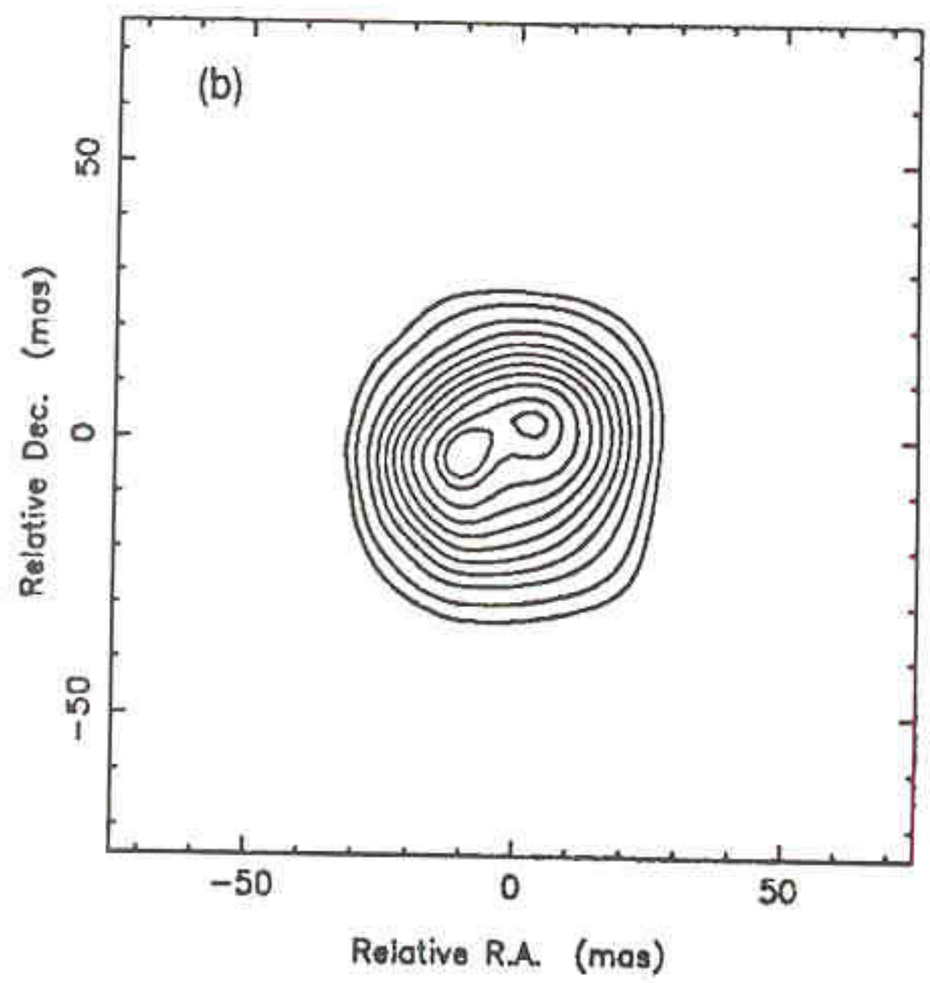

Figure 4. MEM reconstructions of Betelgeuse at 710 nm in (a) 1989 February, and (b) 1991 January. Contours are 5, 10, 20,..., 90, 95 per cent of the peak intensity.

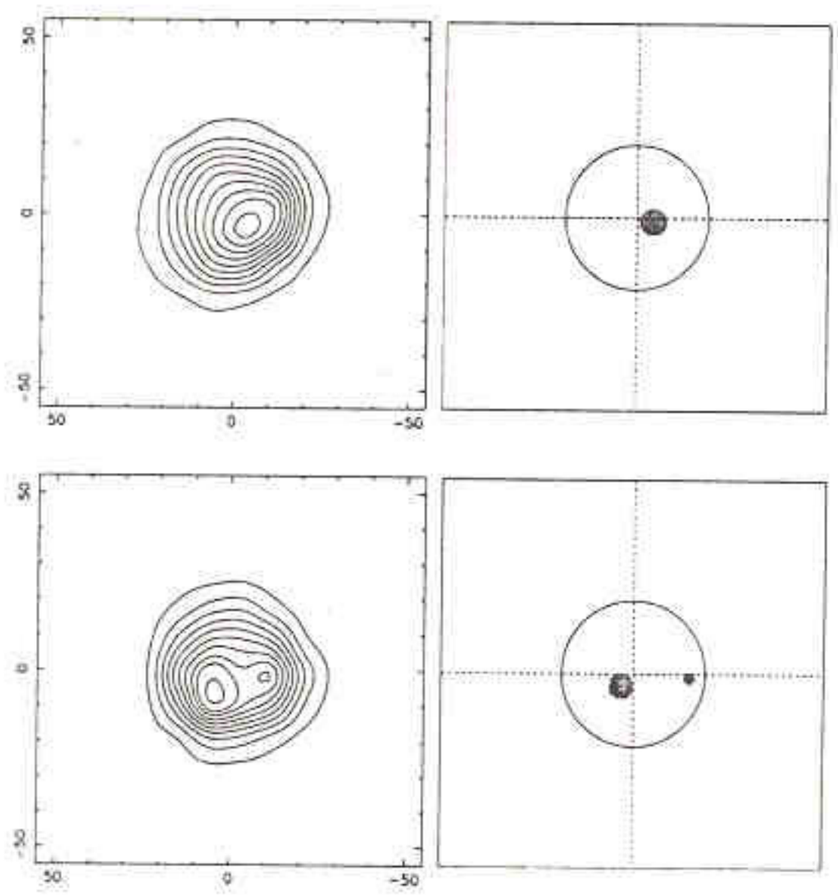

Figure 2. Diffraction-limited image reconstructions of α Her at 633 nm obtained in 1992 July (top) and 1993 June (bottom). These were recovered from the Fourier measurements using an MEM-based self-calibration algorithm. Each image can be represented as the superposition of a uniform disc together with a number of unresolved hotspots. For each image, the right-hand panel shows the locations of the model components, the relative flux of each hotspot being represented by its angular diameter. The contour levels are plotted from 5% to 95% of the peak flux, at intervals of 10%. North is to the top and East to the left. The map scales are in milliarcseconds.

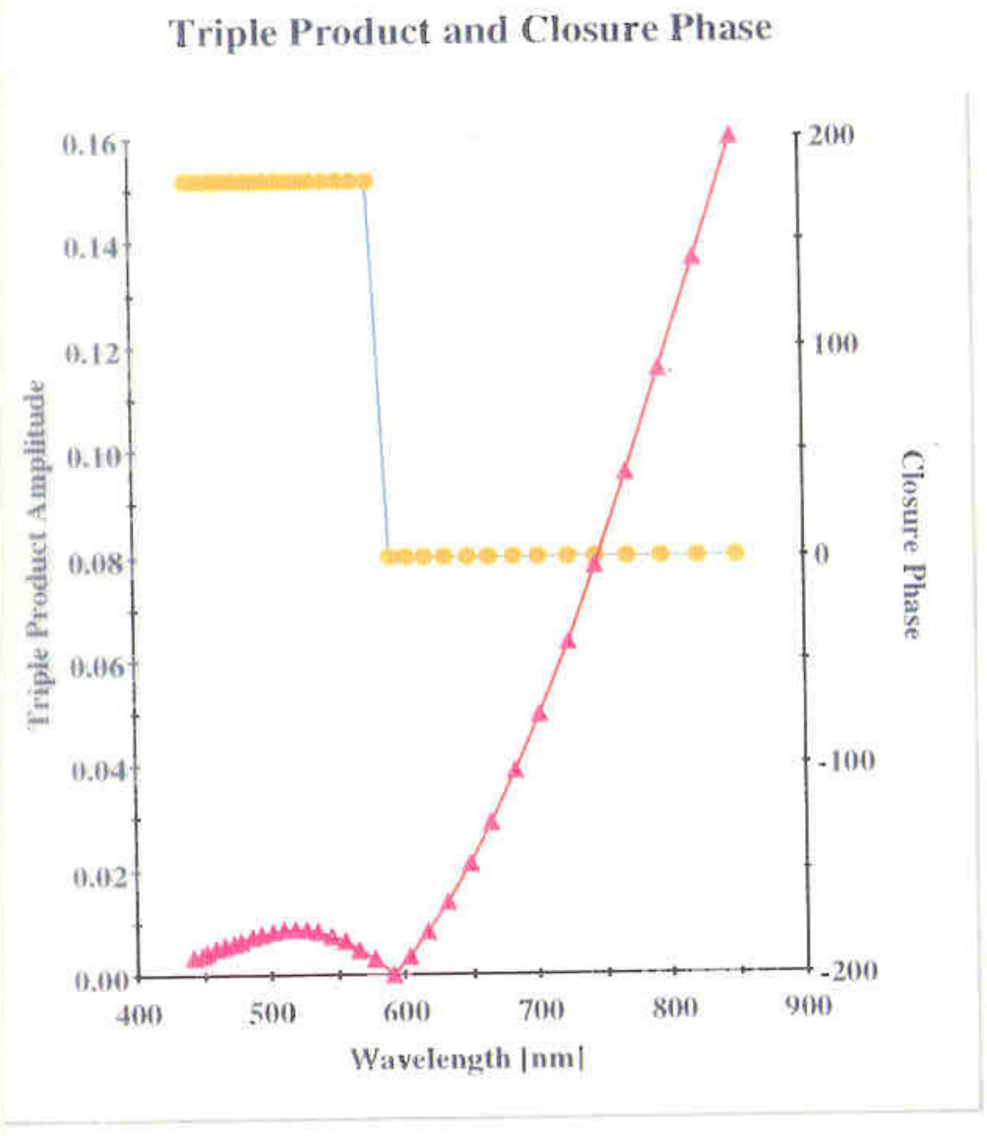

51 Peg

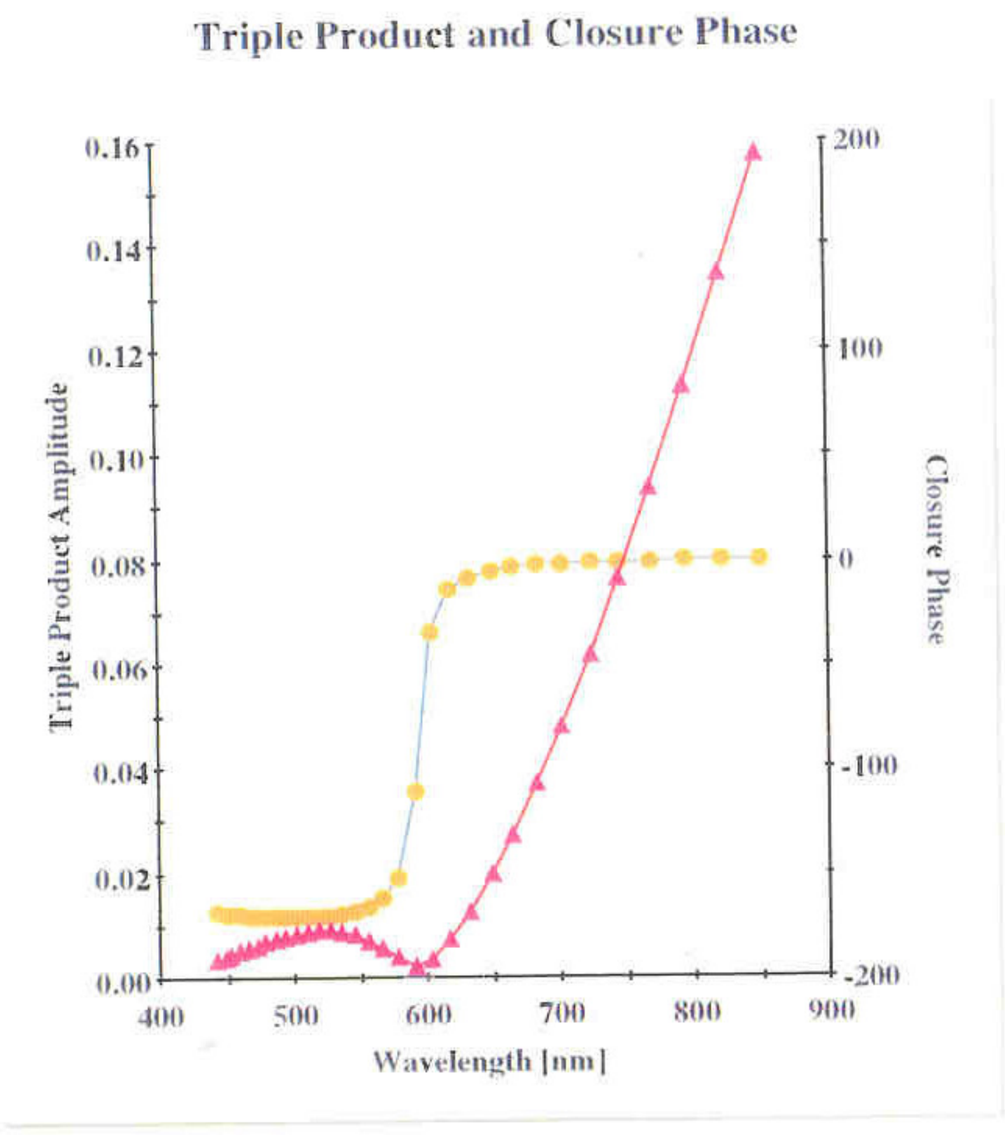

51 Peg with Jupiter Transit

NPOI SIMULATION

- 6 APERTURES = 15 BASELINES

- 32 SPECTRAL CHANNELS

- $32 \cdot 15 = 480$ SIMULTANEOUS VISIBILITIES!

- CONFIGURATION OF ARRAY OPTIMIZED FOR ϕ BOOTSTRAPPING

- FKV0509 = η UMA

$\theta_{LDD} = 12$ mas $\quad T_{EFF} = 5000$ K

$\theta_{SPOT} = 3$ mas $\quad T_{SPOT} = 3500$ K

$\theta_{RB} = 2$ mas

GAUSSIAN NOISE $\sigma = 0.05$

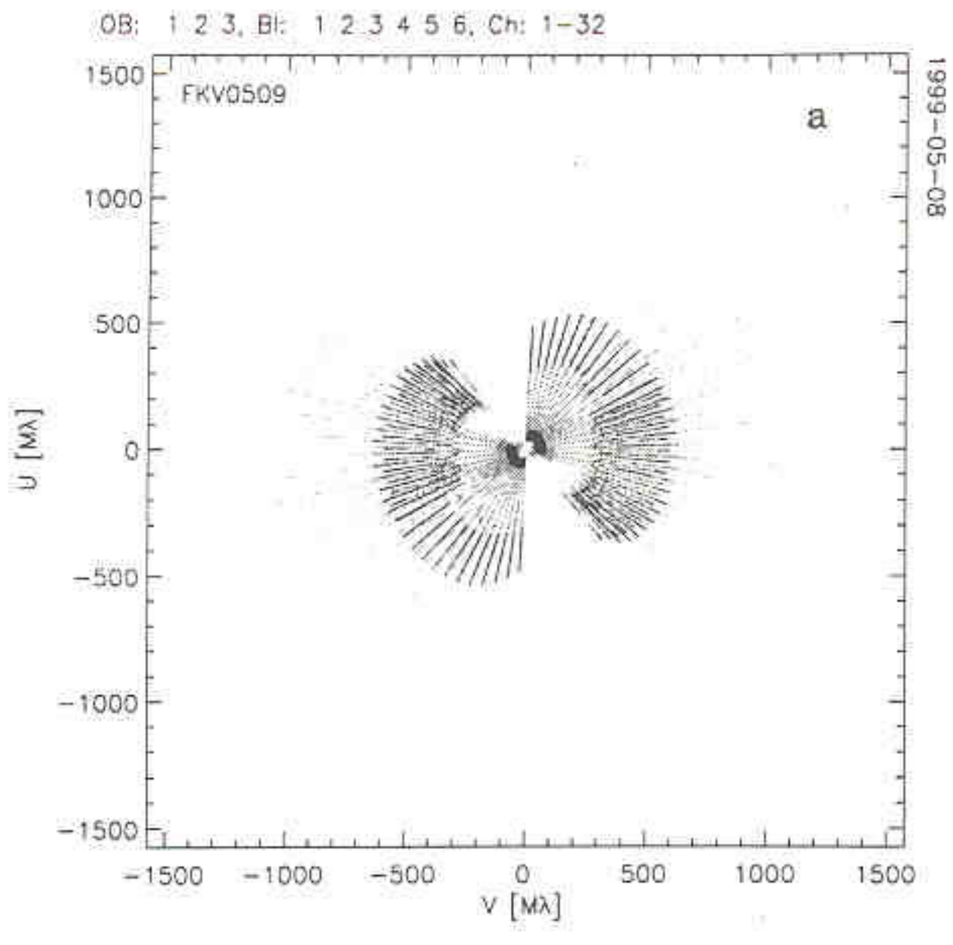

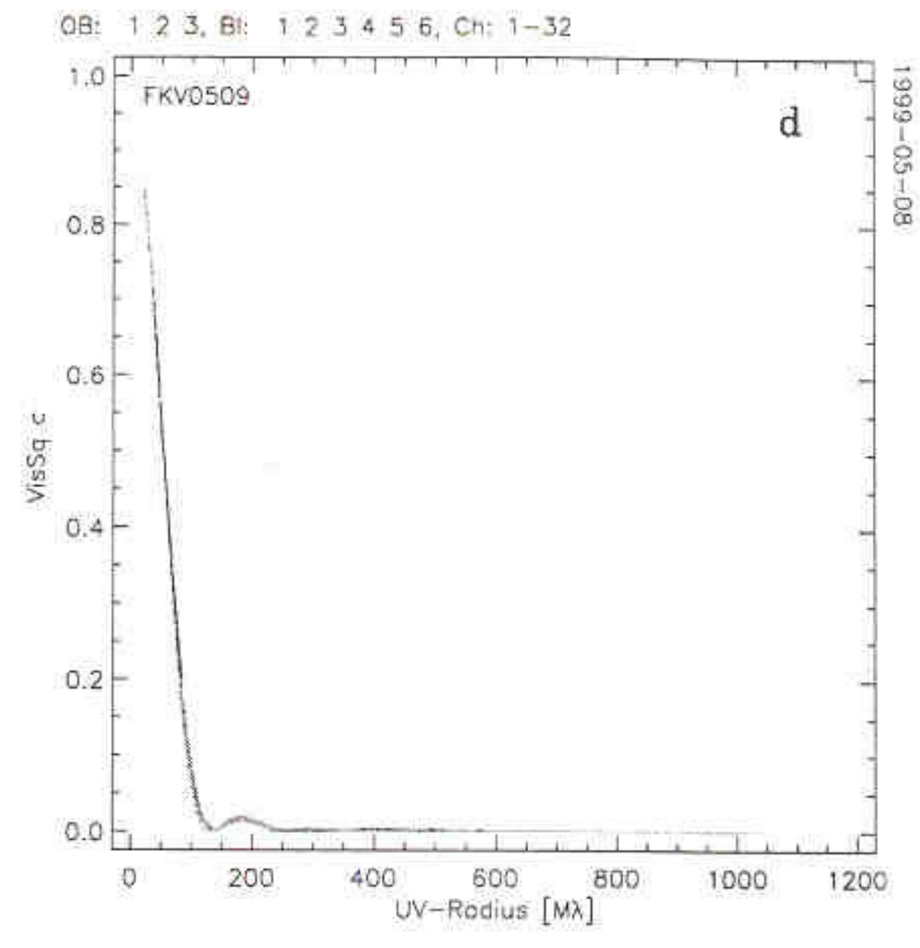

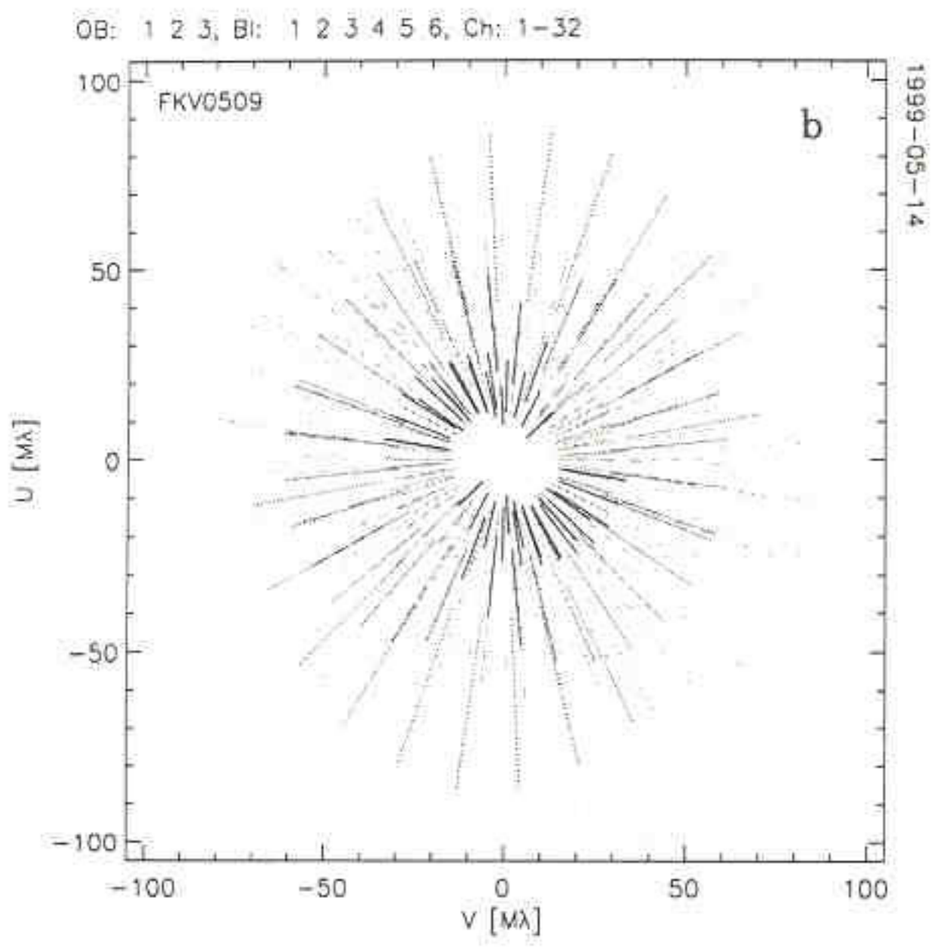

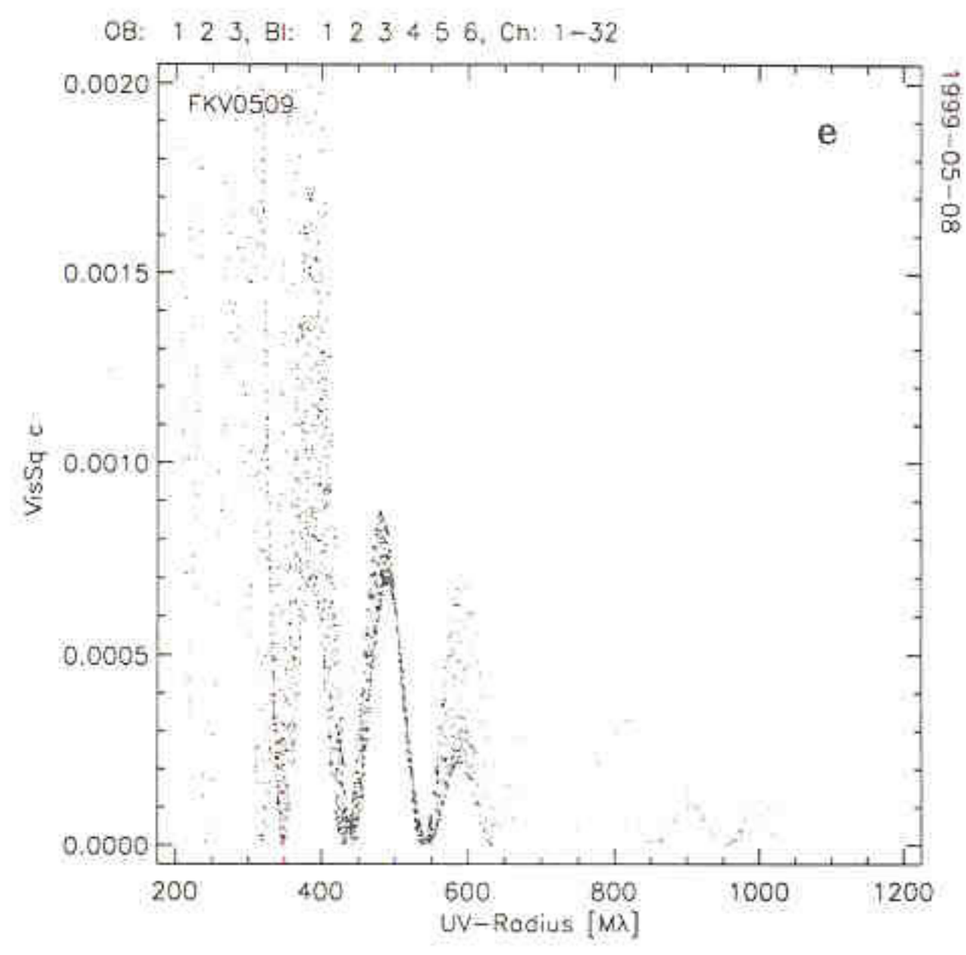

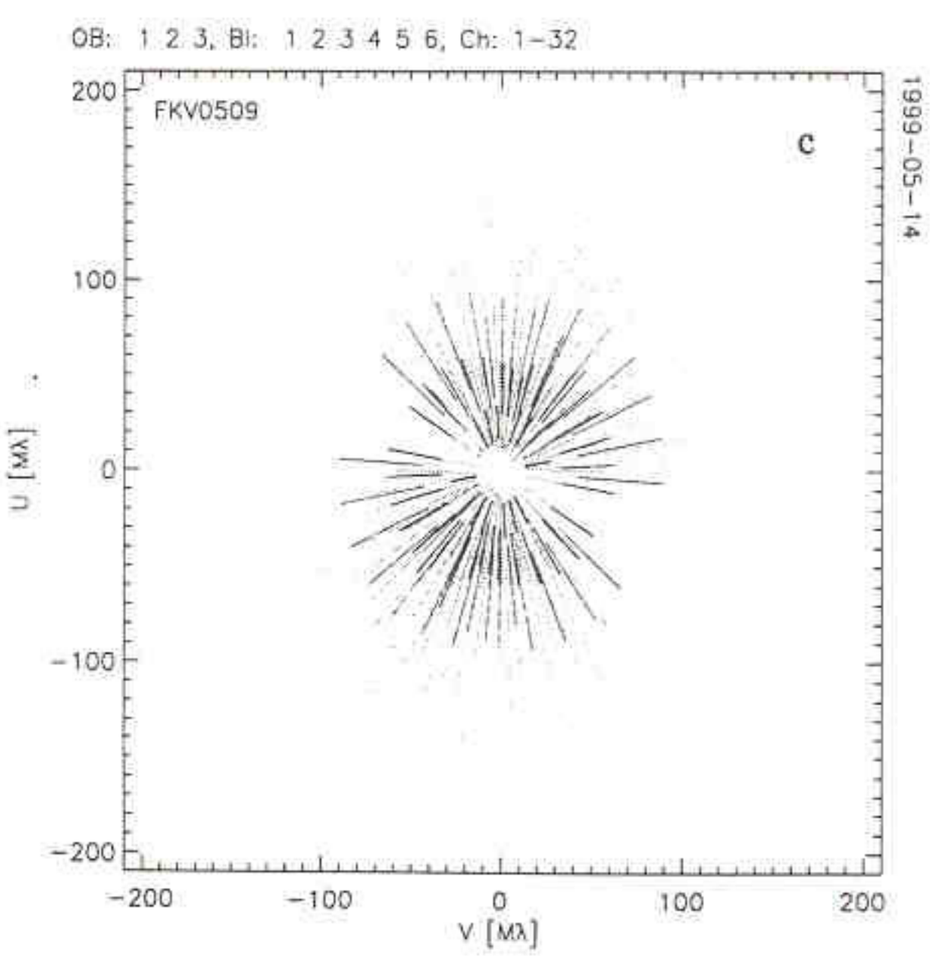

uv-coverages for simulated NPOI observations in a survey configuration (a), and two semi-redundant configurations optimized for stellar surface imaging. Baselines for the latter two can be bootstrapped, i.e. the fringe delays can be computed for the longest baselines from shorter ones, none of which is too long to fully resolve the stellar disk. As is shown in Figs. d and e, the visibility amplitudes drop to very low levels beyond the first NULL, at spacings which contribute information on the small scales of the stellar surface. Such low contrast fringes can not be tracked directly and require semi-redundant arrays. The figures to the left also demonstrate the power of broad band fringe detection in leading to a much impoved uv-coverage. With only a few scans, six stations providing 15 simultaneous baselines, and 32 channels from 450 nm to 850 nm, excellent aperture coverages can be obtained.

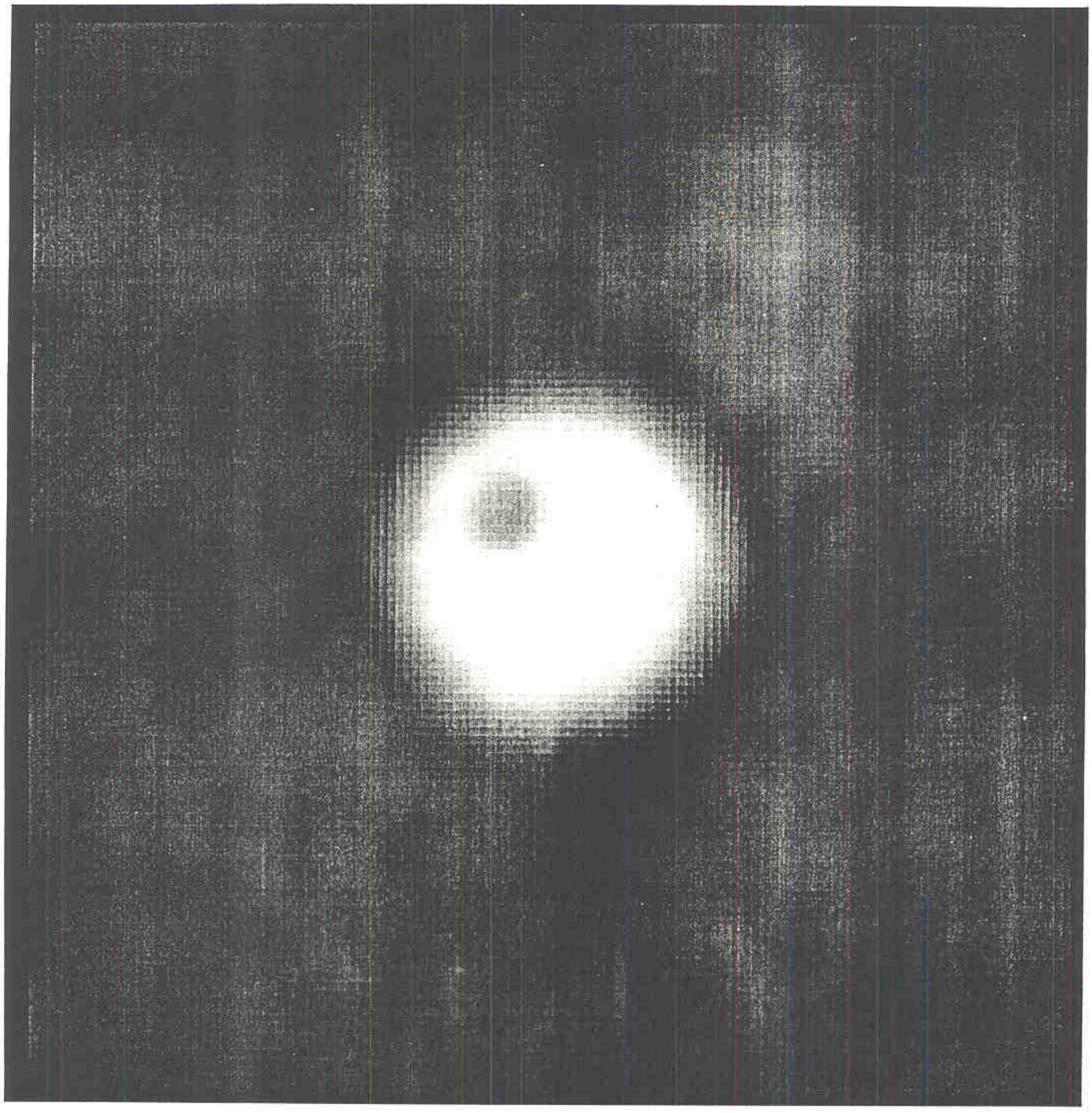

CONCLUSIONS

- EXPECT <u>LOTS</u> OF UDD AND LDD IN THE NEAR FUTURE

- 3 BASELINES >> 3 · (1 BASELINE)

- VACUUM DELAYS HELP ALOT

- CLEVER ARRAY DESIGN HELPS ALOT

- DEDICATED OI ⇒ SPOT DYNAMICS

- TIE-IN BETWEEN NEBULAR HYDRO EVOLUTION & STELLAR MASS LOSS ?